Activity Hierarchy Measurement to Establish Trace Memory-eligible "Primed" Neurons

Yuxin Zhou[1], Liyan Qiu[1], Mark Lyon[2, *], and Xuanmao Chen[1, *]

[1]Department of Molecular, Cellular, and Biomedical Sciences, College of Life Sciences and Agriculture and [2]Department of Mathematics and Statistics, College of Engineering and Physical Sciences, University of New Hampshire, Durham, NH 03824

* Correspondence should be addressed to: Mark Lyon (Mark.Lyon@unh.edu) or Xuanmao Chen (Xuanmao.Chen@unh.edu)

Running Title: Identification of Primed Neurons

Key Words: Memory-eligible Primed Neurons, Memory Formation, Trace Fear Conditioning, *In vivo* Calcium Imaging, Neuronal Activity Hierarchy, Primary Cilia, and Neural Network Simulation

Conflict of Interest Statement: The authors declare that the research was conducted in the absence of any commercial or financial conflict of interest.

Acknowledgements: This study is supported by NIH Grants K01AG054729, P20GM113131, R15MH126317, R15MH125305, COLE Neuroscience Research Awards, and UNH CoRE PRP awards to X.C. Y.Z. is supported by a Summer TA Research Fellowship (STAF) and a Dissertation Year Fellowship (DYF) from UNH Graduate School. We thank Dr. Haiying Wang and the members of the Chen Laboratory for helping to develop this project, and the University Instrumentation Center for A1R HD confocal imaging service.

Abstract

Episodic memory is thought to be preferentially encoded by sparsely distributed memory-eligible "primed" neurons with high excitability in memory-related regions. Based on *in vivo* calcium imaging on freely behaving mice, we developed an analytical method to determine the neuronal activity hierarchy and establish hippocampal primed neurons. Neurons with high activity and memory-associated burst synchronization are identified as primed neurons. When a trace fear memory is being formed or retrieved, the major pattern of the calcium dynamics is predominantly mediated by primed neurons and highly correlated with mouse freezing behaviors. In cilia knockout mice that exhibit severe learning deficits, the percentage of their primed neurons is drastically reduced, and any burst synchronization is strongly suppressed. Consistently, the first principal pattern of cilia knockout neurons does not fully distinguish itself from other minor components or correlate with mouse freezing behaviors. To reveal how a portion of neurons get primed, we developed a numerical model of a neural network that incorporates simulations of linear and non-linear weighting synaptic components, modeling AMPAR- and NMDAR-mediated conductances respectively. Moderate NMDAR to AMPAR ratios can naturally lead to the emergence of primed neurons. In such cases, the neuronal firing averages show a right-skewed log-distribution, similar to the distributions of hippocampal c-Fos expression and the activity levels measured by *in vivo* calcium imaging. In addition, High basal neuronal activity levels speed up the development of activity hierarchy during iterative computation. Together, this study reveals a novel method to measure neuronal activity hierarchy. Our simulation suggests that the accumulation of biased synaptic transmission mediated by the non-linear weighting synaptic component represents an important mechanism for neuronal priming.

Introduction

It is well-known that a small portion of sparsely distributed memory-eligible "primed" neurons (or engram cells) in memory-related regions, including the hippocampus, that mediates episodic memory formation [1-5]. These neurons are recruited to encode memory information and can sustain long-term synaptic modifications to store memories [5,6]. A long-held view on episodic memory formation posits that the memory-eligible neurons "activate" during learning to acquire memory information and the same group of neurons "re-activate" during recall to retrieve the memory [3,4,6,7]. This engram concept was originally proposed over a century ago [8-10], advanced by contextual fear conditioning experiments [3], and supported by engram cell manipulation experiments [4,6,7,11-15].

While the activation and re-activation engram model has greatly advanced our understanding of contextual fear memory and spatial memory [6,12,13,16-18], it has limitations in fully explaining the network mechanisms of episodic memory that does not critically depend on spatial information. First, by detecting the expression of immediate early genes such as c-Fos [3], the "neuronal activation" only captures the cellular step of memory consolidation or the "nuclei activation" of memory-eligible neurons [3], rather than the exact process of memory acquisition. Second, this model does not include the contribution of synaptic components to constructing the neural network of memory. Third, mounting evidence has demonstrated that there is an excitability hierarchy among principal neurons in memory-related regions [19-21]. It is the neurons with increased excitability, namely "primed neurons", in memory-related brain regions [19,22-25] that are preferentially recruited to acquire or retrieve a memory. It has also been documented that the same group of memory-eligible neurons can maintain a high activity status for many days [26-28]. If simply the activation of memory-eligible neurons encoded a memory, it could not allow for the same subset of neurons to encode different memories within the same period. Fourth, our recent deep-brain *in vivo* calcium imaging in conjunction with trace fear conditioning [28] has demonstrated that multiple cycles of aversive foot shock stimuli fails to stimulate relatively "silent" hippocampal CA1 neurons to actively engage in trace fear memory formation. This suggests that it is unlikely for hippocampal principal neurons to directly activate from the silent state to encode a memory. We have also found that the overall activity levels of hippocampal neurons exhibit a right-skewed log-distribution, and a portion of "primed" hippocampal neurons develop burst synchronization when a trace memory is being formed or retrieved [28].

It is recognized that a neuronal activity hierarchy is crucial for hippocampal memory formation [19-21]. However, an *in vivo* neuronal activity hierarchy has yet to be quantitatively determined. Based on deep-brain *in vivo* calcium imaging taken during freely behaving trace fear conditioning experiments, we sought to develop a new method to measure the neuronal activity hierarchy and quantitatively differentiate primed and non-primed neurons. Empirically we have determined two criteria that are the most useful to

distinguish primed neurons from non-primed neurons: (1) high basal activity levels prior to training with increased activity through training; (2) the ability to form memory-associated burst synchronization during trace fear conditioning and recall testing. We included these criteria in our computations. We also employed a novel use of principal component analysis (PCA) to the calcium dynamics of all imaged neurons to extract the major activity pattern, which can then be compared to the calcium dynamics of the primed neurons. We found that primed neurons clearly exhibit distinct features which differentiate them from those of non-primed neurons. To confirm this quantification methodology, we also used a strain of primary cilia knockout mice which exhibit severe learning deficits. As expected, cilia knockout mice have a lower activity hierarchy and much fewer primed neurons, do not develop memory-associated burst synchronization, and do not form a major pattern associated with training that can be fully distinguished from other minor patterns

To date, little is known about how a neural activity hierarchy is developed to enable a fraction of neurons to be preferentially recruited to encode a hippocampal memory. To explore the mechanisms of neuronal priming, we developed a simplified neural network simulation model that consists of a two-dimensional array of neurons. It incorporates simulation of synaptic transmission that has linear and non-linear weighting components. Linear and non-linear weighted components simulate the AMPAR- and NMDAR-mediated conductances, respectively, in the post-synapses. One crucial difference between the AMPAR- and NMDAR-mediated conductances is the voltage-dependent magnesium-blockade of the NMDAR[29,30]. In addition to glutamate binding, NMDAR requires the depolarization of membrane potential to unbind the magnesium blockade and fully open the ion channel [30,31]. This means that NMDARs in active or depolarized neurons are more responsive to glutamate stimulation than those in inactive neurons, thereby generating a non-linear weighting component of the excitatory synaptic transmission. This scenario favors effective synaptic communication to active (or depolarized) neurons over inactive neurons. Our simulation shows that the presence of NMDAR is critical for the development of neuronal priming and a moderate ratio of NMDAR to AMPAR can naturally lead to the emergence of primed neurons in the course of 12,500 computational iterations. In such cases, the overall neuronal firing averages show a right-skewed log-distribution, similar to the right-skewed distribution measured by c-Fos expression and by our *in vivo* calcium imaging [28]. We further found that the basal neuronal activity also affects the development of the neuronal activity hierarchy and that a high initial neuronal activity speeds up the formation of the activity hierarchy. This simulation is the first to show that the accumulation of non-linear synaptic transmission, likely mediated by the NMDAR conductance, represents an important mechanism for neuronal priming.

Methods

Mice

All animal-related procedures were approved and conducted in accordance with the guidelines of the Institutional Animal Care and Use Committee of the University of New Hampshire. Mice were maintained on a 12-h light/dark cycle at 22°C and had access to food and water ad libitum. The Ift88 floxed mouse strain [32] was cross-bred with UBC-Cre/ERT2 as previously reported (C57B1/6j genetic background, mixed genders) [33]. At the age of 8-10 weeks, Ift88 flox/flox: UBC-Cre/ERT2 mice were orally administrated with tamoxifen (0.2 mg/g body weight, consecutive 7 days) to induce Cre recombinase expression to ablate Ift88 and generate Ift88 cilia KO mice, or with vehicle (corn oil) to make vehicle control mice. Ift88 flox/+ (or Ift88 +/+): UBC-Cre/ERT2 mice with the same tamoxifen treatment were used as genotype controls. We observed that vehicle control and genotype control mice exhibited very similar results and their data were combined into one control group. Ift88 cilia KO mice exhibit normal acoustic and foot-shock responses. To verify that primary cilia were efficiently deleted in cilia KO mice, we also assessed the efficiency of cilia ablation with immunostaining using AC3 antibody (1:4000, Cat# RPCA-ACIII, EnCor). More than 90% of primary cilia in the hippocampus were ablated (see Fig. 2A) using this inducible ablation protocol, consistent with our prior report that deleted AC3 [33]. For behavioral tests, mice were handled by investigators for 5 days to allow them to adjust to the investigators before starting the experiments.

Mice surgery and AAV viral vector injection

Surgery was performed one week after tamoxifen/vehicle administration, as previously described[28]. Mice were anesthetized by 1.5-2% isoflurane and mounted on a stereotaxic frame (David Kopf Model 940). A special canula implant (Mauna Kea Technologies, Paris, France) was installed above a small window through the skull (coordinate: AP: −1.95 to −2.05 mm relative to the Bregma, ML: −1.6 mm relative to the midline). The cannula implant allowed the injection of viral vector (0.5 µl AAV1-Syn-GCaMP6m, Addgene, ID 100841) into the hippocampal CA1 region (coordinate: DV: −1.45 to -1.55 mm from the skull) to express calcium indicator and allow a fiber-optic imaging microprobe to go through (Fig. 1A, Created with BioRender.com.). Mice were used for *in vivo* calcium imaging and trace fear conditioning 8 weeks after the canula implantation surgery.

Imaging acquisition

In vivo calcium dynamics were acquired by a Cellvizio Dual-Band 488/660 imaging system (Mauna Kea Technologies, Paris, France). A CerboflexJ NeuroPak deep-brain fiber-optic microprobe (having over

7600 optical fibers) collected the green florescent signal of GCaMP6m from hippocampal CA1 region (coordinate relative to the Bregma: AP: −1.95 to −2.05 mm, ML: −1.6 mm, DV: −1.75 to -2.55 mm). GCaMP6m fluorescent signals were acquired every training or recall cycle to monitor the real-time calcium dynamics. Imaging sessions were also recorded prior to training and recall, after training, during resting and under isoflurane-induced anesthesia. Acquired imaging data (25 Hz, 66 seconds for training cycles, 55 seconds for others) were analyzed off-line using IC Viewer 3.8 (Mauna Kea Technologies, Paris, France). Regions of interest (ROI) of the calcium signals for individual cells were manually selected to cover at least 3 fibers. ROIs from background areas covering 50 fibers without GCaMP6 expression were selected to detect the background pattern, which, in turn, was used to eliminate imaging noise and artifacts. 70 - 140 individual cell ROIs and 12 background ROIs were collected from every animal (Fig. S1C). Representative calcium traces throughout the manuscript are the calcium intensity relative to the basal level (%ΔF/F) computed as the GCaMP6m fluorescence intensity divided by the intensity average of 1 second (25 frames) before tone for every recording. All calcium traces used for computing synchronization and other analysis were first transformed to 5-second moving SD traces and the background artifacts were removed (Fig. 1K and Fig. S1).

Background noise elimination

The lightweight of the fiber-optic imaging microprobe permits animals to behave freely. However, free behaving imaging may generate certain motion artifacts and background noise. To detect background imaging noise, 12 background ROIs were selected from areas without GCaMP6 expression (Fig. S1C). Any consistent fluctuations in these background ROIs were considered imaging noise or motion artifacts (Fig. S1D). To remove any background noise patterns, the calcium traces from the background regions were first transformed by computing a standard deviation over a 5-second moving window (Fig. S1D). While the SD trace over a 5-second window does “smear” the data over those 5-seconds, this has the benefit of reducing the effect of any white noise in the data in addition to eliminating potentially spurious phase information (Fig. S1A-B). The final calculations are not particularly sensitive to the precise choice in the length of the window as long as the same process and window lengths are used for both the background regions and the individual neurons. The background 5-second SD traces were normalized and then analyzed through a PCA analysis, which is used to identify any patterns consistent among the background regions (Fig. S1D-ii). The principal components in the PCA analysis with scores that were above the average (approximately 4-5 patterns) were then deemed to be artifacts in data and were used as the background artifact/noise patterns (Fig. S1D-iii). The identified artifacts were then eliminated from all individually neuronal calcium signals’ 5-second SD traces (Fig. S1E-F) by calculating the projection

of the individual signal patterns onto the identified artifact patterns and subtracting that projection from the individual neuron's SD trace, thus orthogonalizing all the individual neuron's SD traces to all artifact patterns (Fig. S1F).

PCA analysis and the calculation of the neural synchronization levels

Once the 5s-moving SD trace of each individually measured neuron had been computed and all artifact patterns removed, a second PCA was performed to determine the major pattern in the individual neuron responses. Here we looked at the singular vector with the largest singular value (or the principal component with the largest score) which represents a signal pattern that was exhibited more often in the neurons than any other pattern. Since this major pattern was constructed after the SD traces of all the individual neurons have had any background artifacts removed, the major pattern is orthogonal (or completely uncorrelated) to any of the identified background artifacts patterns (Fig. S1F).

After the major pattern for neuronal signals has been identified, correlations between the SD traces of all individual neurons and the major pattern can be computed (results reported in Fig. 4A). Similarly, the correlation between any given pair of SD traces can be computed in the heatmaps (results reported in Fig. 3). Values for these correlations which are above 0.7 signify strong correlations [34]. When the principal component score corresponding to the major pattern was significantly larger than the next largest score, many individual SD trace signals were found to have high correlations in our imaging data (Fig. S2). These high correlations with a single major pattern are a clear indication of neural priming. The extent to which the neuron is primed can be estimated by the number of neurons exhibiting a strong correlation with the major pattern.

We collected calcium images of individual neurons under different conditions, including under anesthesia using 2% isoflurane. The neuronal calcium dynamics under anesthesia served as the internal reference for normalization, used to eliminate individual variance in signal detection and GCaMP6m expression and to allow for quantitative comparison between different animals. The activity levels of individual neurons were calculated as the ratio of the SD-of-SD value during training cycles to the SD-of-SD value under anesthesia. In our previous report [28], the neuronal activity levels were estimated using the ratio of variances of the calcium traces during training relative to those under sleep (Fig. S3B). That method could distinguish silent neurons from primed neurons clearly but was unable to accurately separate intermediately active neurons from primed neurons (Fig. 4B). We define primed neurons as high-activity neurons with strong responses to learning cues and able to form burst synchronization with each other. Some intermediately active neurons be exhibit relatively high activity but while their calcium traces showed consistent high amplitude, they were not as responsive to learning cues in that their SD traces

remained relatively uncorrelated with the major pattern (Fig. S1B). The second order activity level measured by the SD-of-SD more accurately separates primed neurons from intermediately active neurons than the first order activity level measured by variance. Using the SD-of-SD value highlights, in particular, bursting signals and using it we can differentiate bursting signals from consistent high-amplitude fluctuations and efficiently distinguish primed neurons from intermediate and silent neurons (Fig. 4C).

Immunofluorescence staining

Mice were euthanized, and brain tissues were extracted and fixed with 4% paraformaldehyde at 4°C overnight. After sliced, brain samples were subjected to fluorescence immunostaining using primary antibodies against ACIII (1:4000, Cat# RPCA-ACIII, EnCor), GFAP (1:500, Cat# Z0334, Dako), and c-Fos (1:500, Cat# MCA-2H2, EnCor), followed by secondary antibodies (conjugated with Alexa Fluor 488, 546, or 647, 1:500) to verify GCaMP6 expression, imaging site and c-Fos expression, reactive astrogliosis (GFAP staining) in the hippocampal CA1 region. The number of c-Fos positive neurons normalized to the nuclear number and GFAP/DAPI intensity ratio were compared between the surgical and non-surgical hemispheres in 12 slices collected from 4 animals.

Control mice (n = 5, including vehicle control and genotype control at nine weeks after tamoxifen/vehicle administration) were euthanized 45 minutes after trace fear conditioning following the protocol above. Sliced brain samples (50μm) were subjected to fluorescence immunostaining using primary antibodies against c-Fos (1:5000, Cat# RPCA-c-Fos, EnCor) and secondary antibodies (conjugated with Alexa Fluor 488, 1:500) to measure neuronal activity level in the hippocampal CA1 region. The fluorescent intensity of c-Fos signal from the single cell was compared to the average of all c-Fos positive neurons in the same image for the neuronal activity level distribution. All fluorescence images were captured using a Nikon A1R HD confocal microscope acquired using the same setting including exposure time, gain and laser power settings. Images were processed and analyzed by Fiji ImageJ [35].

Electroencephalogram (EEG) surgery and recording under isoflurane-induced anesthesia

Mice at 3-4 months old age (mixed sexes) were implanted with EEG/EMG headmounts, performed as described previously [36] and followed the manufacturer's instructions (Pinnacle Technology, Lawrence, Kansas). Briefly, mice were anesthetized by isoflurane before being aligned in a stereotaxic surgery apparatus. After exposing the mouse skull surface, headmount was centered along the sagittal suture, with its front edge 3.5 mm anterior to bregma. EEG headmount was secured to the skull with stainless steel screws, which also served as EEG electrodes. After a one-week recovery from surgery in home cages,

mice were tethered to EEG commutators and housed in circular cages individually. Mice were adapted to the EEG connecting wire in a free-moving condition for 2 days. Afterwards, mice were subsequently put in a closed chamber containing 3% isoflurane to monitor EEG brain waveform over the course of anesthesia. EEG was amplified 5,000 times and sampled at a rate of 400 Hz. EEG waveforms were analyzed using Sirenia software offline (Pinnacle Technology, Lawrence, Kansas).

Trace fear conditioning test

Trace fear conditioning was performed using Ift88 cilia KOs and controls 8 weeks after tamoxifen/vehicle administration. The mouse was placed in a fear conditioning chamber (VFC-008CT-LP) with a grid floor (VFC-005A, Med Associates Inc, Vermont). Trace fear conditioning was conducted as previously described [28] after 10 minutes of exploration and acclimation with minor modifications. A neutral tone (3 kHz, 80 dB, 15 s) was used as a conditioning stimulus, followed by a mild electric foot shock (0.7 mA, 1 s) as an un-conditioning stimulus. There was a 30 s trace period between tone and shock to slow the direct association between CS and US. The training cycle (10 s prior to tone, 15 s tone, 30 s delay, 1 s foot shock, 10 s post shock, and 190 s interval) was repeated 7 times to form a trace memory. The video was recorded for 20 mins after the 7th training cycle to monitor the difference of mouse prior- and post-training behaviors. After the training procedure, the mouse was placed in a resting box with *ab libitum* bedding and feeding. Normal mouse behaviors, including nesting, grooming, feeding, and drinking, sleeping, were observed during a 2-hour resting period. Afterward, memory retrieval was tested by recall procedure in a new environment (solid plastic walls and floor) after 10 mins of exploration and acclimation. A modified tone (3 kHz, 80 dB, 5 s) was used as the cue for recall. The recall cycle (10 s prior to tone, 5 s tone, 30 s delay, absence of foot shock, 10 s post shock, and 110 s interval) was repeated 5 times. Trace fear conditioning training and recall procedures were videotaped (25 frames per second). Videos were tracked by Noldus Ethovision XT (version 11.5) for real-time moving velocity, freezing, and locomotion. Freezing was defined as real-time velocity lower than 1 mm/s, automatically measured by Enthovision XT. 10 pairs of cilia KOs and controls (mixed genders) were used for comparison in the trace fear conditioning test.

Morris water maze test

A behavioral paradigm of the Morris water maze test was used to determine if cilia KOs exhibit impaired spatial memory. A 150 cm-diameter circular pool was filled with 25 cm-deep water (23 ℃) with white tempura paint. Four shapes (square, circle, triangle and star) were labeled in the cardinal directions of the tank periphery as start points. A 10 cm-diameter circular platform was hidden 1.5 cm below the water surface in the target quarter. Three 120-second trials from different start points were conducted daily for

5 consecutive days. When a mouse failed to find the hidden platform within 120 seconds, it would be placed on the platform for 20 seconds. One day following training, mice were put back into the tank without the hidden platform for 120 seconds in the probe test (4 trials in the 6th day). The trials were videotaped (25 frames per second). Noldus Ethovision XT (Version 11.5) was used to track the latency to find the hidden platform, velocity, and duration in every quarter. Means of daily trials were compared between 10 pairs of (mixed genders) cilia KO and control mice.

Bursting analysis of time-frequency plots of imaging

While SD traces only capture the magnitudes of fluctuations in the signal, some information on the frequency of the fluctuations can be obtained. The maximum frequency that can be directly observed is limited to 12.5 Hz (due to the 25 Hz sampling rate) while any higher frequencies will be aliased and appear as a frequency from 0 to 12.5 Hz. Time-frequency plots were generated by computing short-time Fourier transforms using the "stft" algorithm in MATLAB. The fast Fourier transform (FFT) length was set to 512 with an overlap of 252 and a 256 length Kaiser-Bessel-derived window with a parameter beta of 10. The frequency as function of time can then be displayed as a heat map (results in Fig. 3). Synchronization and bursting patterns can still be observed even if the frequency data is aliased and the precise frequencies in the signal exhibiting the bursting behavior cannot be determined.

Neural network simulation

A two-dimensional computational array of $N_r = 2000$ rows (cell number per layer) by $N_c = 30$ columns (or layers) of neurons was simulated through 12,500 computational iterations. The model serves as a relatively simple demonstration of a possible mechanism for neural priming. As the precise configuration of a grouping of neurons in the brain is unique and extremely complex, many simplifying assumptions were made to make the simulation tractable, though extensions and generalizations of this model will be explored in future work. The parameters used in the model were modified through trial and error to obtain the results shown, and using different parameters can yield significantly different results and distributions, although alternate parameters can also yield similar results.

Several properties are kept track of for each neuron at each time cycle. The activation level of the neuron in the i^{th} row and the j^{th} column is labeled A_{ij}, representing the activation level of the neuron. The net charge in the neuron was scaled to a unit interval so that if A_{ij} reaches or exceeds the value of 1, the neuron will fire which will result in a charge being received by neurons in column $j + 1$. The value F_{ij} is the amount a given neuron has fired over approximately the last $2{,}500$ time cycles and represents the

recent firing activity level of the neuron. To accelerate the simulation, F_{ij} was updated once every 50 iterations. This simulation was initialized with all values of A_{ij} randomly and uniformly selected from the interval [0,1] and all values of F_{ij} set to zero. A given neuron in layer j is assumed to be connected to all the neurons in layer $j+1$ (that is when a neuron in layer j fires, the activation level of all 2000 neurons in layer $j+1$ will increase to varying degrees). The connection strength, S_{ki} between a neuron in layer j and row i to a neuron in layer $j+1$ and row k is independent of j and given by

$$S_{ki} = \frac{e^{-0.003D_{ki}}}{\sum_k e^{-0.003D_{ki}}},$$

where D_{ki} is given by the minimum of three quantities $|k-i|$, $|k-i-N_r|$, and $|k-i+N_r|$. These definitions enforce a periodic boundary condition so that the bottom row is considered to be just above the top row. While a given neuron in layer j does connect to all neurons in layer $j+1$, S_{ki} decays rapidly as the rows k and i become further separated and so each neuron in layer j will only have a strong connection with a relatively small number of neurons in layer $j+1$ (less than 100).

At the beginning of each cycle, 120 neurons (6%) were randomly selected from the first layer and the corresponding values for the activation level of those 120 neurons were set to 1. Then, layer by layer, the entire mesh is checked to see if $A_{ij} \geq 1$ and all the neurons with an activation level greater than or equal to 1 are fired, before moving on to the next layer.

As each neuron fires, two separate calculations for the signal transmission are computed, modeling the production and transmission of neurotransmitters, being passed to the next layer.

For the linear AMPAR-mediated synaptic conductance, when the neuron in row i and column j fires, the activation levels for the neurons, $A_{k(j+1)}$ for all k, are increased by an amount

$$A_{k(j+1)} = A_{k(j+1)} + 0.725A_{ij}S_{ki}.$$

This increase is only affected by the strength of the connection between the neurons and is independent of the activity level of any neuron. A secondary, non-linear synaptic NMDAR-mediated conductance for all k is calculated as

$$A_{k(j+1)} = A_{k(j+1)} + \frac{0.275A_{ij}S_{ki}\left(f(F_{k(j+1)}) + 0.00001\right)^2}{\sum_k A_{ij}S_{ki}\left(f(F_{k(j+1)}) + 0.00001\right)^2},$$

where the function f is a monotonically increasing form of a logistic function given by

$$f(x) = \frac{\frac{1}{1+e^{-0.015(x-250)}} - \frac{1}{1+e^{3.75}}}{\left(1 - \frac{1}{1+e^{3.75}}\right)}.$$

The logistic function guarantees that as the firing activity level of the target neuron increases, so does the proportion of the charge that neuron receives up until the point where the NMDAR gates can be considered effectively fully open at which point $f(x)$ will be equal to 1. For example, $f(600)$ and $f(700)$ have nearly identical values and both are extremely close to 1. The value 0.00001 is merely chosen as a small value that will generally have little impact on the calculation but prevents the denominator from being 0 before any neurons have fired.

The two transmissions of charge above, corresponding to AMPAR- and NMDAR-mediated conductances (net of any impendence), respectively, together sum over k to be precisely the value of A_{ij} which ensures the stability of the algorithm. If they summed, in general, to be greater than A_{ij}, then in each subsequent layer the number of times the neurons will fire grows exponentially and unphysically. If they summed, in general, to be less than A_{ij}, then in each subsequent layer the number of times the neurons will fire shrinks exponentially and neurons may almost never fire in the furthest layers, which is also unphysical. After the values of $A_{k(j+1)}$ have been updated, the value of A_{ij} is set to zero and the algorithm moves on to the next neuron to fire. For neurons firing in the last layer, there is no transmission, and we need only to set A_{ij} to zero. The AMPAR conductance does not depend on how active any neuron is, while the NMDAR conductance increase as the receiving neuron becomes more active relative to the other connected neurons. Even though the NMDAR conductance is only 27.5% of the total, this is sufficient for neural priming to be observed.

Statistical analysis and graphic data presentation

If the data's sample sizes were more than 50, or if the sample size were less than 50 but they passed normality tests, statistical analyses were carried out using Student's *t*-test for a two-group comparison, or ANOVA test for multiple-group comparison. If the data's sample sizes were less than 50 and they failed to pass normality tests, a nonparametric test was used for two-group comparison or for multiple-group comparison. ns, not significant, *P < .05, **P < .01, ***P < .001, and ****P < .0001. A difference in data comparison was considered statistically significant if P < .05. Values in graphic data presentation are shown as the means ± the standard error of the mean.

Results

One-day fiber-optic *in vivo* calcium imaging avoids pathological neuronal activation, uniquely suited to determine neuronal activity hierarchy.

It is critical to ensure no pathological neuronal activation before *in vivo* calcium imaging, as this helps maintain neural activity at the physiological state to allow for the determination of the neuronal activity

hierarchy and the quantitative identification of primed neurons. We combined a deep-brain fiber-optic confocal (FOC) fluorescence endomicroscopy with mouse trace fear conditioning experiment in a time-locked manner. One limitation of this imaging system is that although it can maintain imaging stability for over 7 hours, it does not permit repetitive imaging for multiple days [28]. However, this instant one-day imaging approach instead confers one advantage: it omits the need for GRIN lens implantation into the brain and thereby avoids pathological activation and hippocampal inflammation caused by GRIN lens implantation and tissue injury (Fig. 1A). Indeed, the mouse hippocampus did not display pathological activation weeks after canula installation surgery and AAV injection, as evidenced by comparable c-Fos expression and GFAP staining in the surgical and non-surgical hemispheres (Fig. 1B-E). In contrast, 2-3 days after completion of imaging, GFAP expression was found to be strongly elevated in the imaged region, compared to the non-imaged hemisphere (Fig. 1F). This demonstrates that the mouse hippocampus can stay very close to the physiological conditions right before imaging, but not after imaging that could cause certain injury.

The imaging microprobe has an inner diameter of 300 μm, encasing a bundle of ~7600 optic fibers of 1 μm. It has a lateral resolution of 3 μm, which allowed for tracking calcium dynamics at a cellular resolution [28]. We also developed several empirical strategies to ensure that our imaging data was collected from single cells (Fig. 1H-J). ROIs encircling multiple fibers (minimal 3 fibers) (outer part, red) or 1 fiber (inner part, green) were manually drawn respectively, and their calcium traces were compared. 1-fiber ROIs covered a smaller, central part of the soma, whereas multiple-fiber ROIs covered a larger area (~ 7 x 10 μm) (Fig. 1I). The fluorescence intensity at the center is brighter than the edge, which helped separate the two neurons. We also compared active neurons with several relatively inactive neurons surrounding it. During training, neural synchronization occurs among active neurons which generally seat distantly, and rarely among neighboring neurons (Fig. 1I). We mostly used multiple-fiber ROIs data in our subsequent analysis because this yielded a better signal-to-noise ratio (Fig. 1I). However, multiple-fiber ROIs may potentially cover a region covering two neurons. To address this, if a multiple-fiber ROI's activity pattern was very similar to all individual 1-fiber ROIs within the area, we deduced that the multiple-fiber ROIs cover a region from the same neuron as those 1-fiber ROIs (Fig. 1J). If the activity pattern of multiple-fiber ROI was different from individual 1-fiber ROIs, we reasoned this multiple-fiber ROI may cover a region for more than one neuron (Fig. 1J), whose data were then excluded in our analysis, or the ROI could be re-drawn until a single neuron was clearly defined. Further, we excluded imaging regions if two neurons' imaging intensity contrast could not be clearly separated. Hence, we were able to collect imaging data from ROIs of single neurons and exclude ROIs that cover more than one

neuron. Together, this deep-brain imaging at the cellular resolution in freely behaving mice free of prior pathological activation is well-suited to determine hippocampal neuronal activity hierarchy *in vivo*.

Fluorescent traces of cellular calcium signals were collected and transformed into 5 second moving standard deviation (SD) traces, followed by artifact/noise elimination, then compute synchronization levels and perform other statistical analysis (Fig. 1K). More specifically, we first converted neuronal calcium traces into 5-second moving SD traces to smooth white noise and amplify bursts (Fig. S1A-B). Next, we calculated the projection of the individual neuronal SD traces onto the identified background noise patterns (which result from PCA to the SD traces of 12 background ROIs), and subtracted that projection from individual neuron's SD traces, thus orthogonalizing individual neuron's SD traces to all background patterns (see Method and Fig. S2C-F). After eliminating background patterns, the SD traces of individual neurons were used for the subsequent statistical analysis, including extracting synchronized patterns among all neurons (or among selected neuron groups) to generate the major pattern of the PCA, to compute the synchronization levels of individual neurons with the major pattern (Fig. 3), to calculate the correlation between mouse freezing behaviors and the major pattern (Fig. 4), and to compute the SD-of-SD that reflects neuronal activity levels (Fig. 5), as well as sort out primed neurons using synchronization levels and the SD-of SD values (Fig. 6).

Ift88 cilia KO mice exhibit severe deficits in spatial learning and trace fear conditioning and suppressed EEG waveform activity.

To help verify our methods to determine neuronal activity hierarchy and determine primed neurons, we used Ift88 cilia KO mice (Ift88 flox/flox; UBC-Cre/ERT2 mice), which represent a temporally induced primary cilia loss-of function animal model [32,37] (Fig. 2A). We subjected cilia KO and control mice to a trace fear conditioning test and trained animals to associate the innocuous tone with aversive mild electric foot shock. During training, control animals had a markedly increased freezing score starting from the 3rd or 4th training cycle, consistent with previous reports [28]**,** whereas cilia KOs displayed a much slower response to training. Cilia KOs displayed significantly reduced freezing behaviors during the trace period of the 7 training cycles (Fig. 2B). Aversive memory formed during the conditioning can last several minutes. We compared cilia KO and control mouse freezing behaviors for 10 minutes after training relative to 10 minutes prior to training. Trace conditioning significantly increased the relative freezing of controls, but not cilia KOs (Fig. 2C). In recall testing, cilia KOs also displayed weaker tone-reduced freezing than control mice (Fig. 2D). This data indicate that cilia KO mice exhibit severe deficits in associative learning.

Next, we subjected the mice to a Morris water maze test to evaluate their ability to form a spatial memory. In the Morris water maze test, all mice had 5 days of training with a hidden platform at a fixed position. During these training days, control mice showed significantly decreasing escape latency every day, whereas cilia KOs performed much worse (Fig. 2E). In the subsequent probe test, control mice revealed a high preference for the target quarter than other quarters, whereas cilia KOs were unable to distinguish the 4 quarters (Fig. 2F-G). These data demonstrate that cilia KOs exhibit impaired spatial navigation.

To monitor if the general electrical activity in cilia KOs is suppressed, we used the mice for the EEG recording and induced them to reach the isoelectric (brain-death) anesthetic stage using 3% isoflurane. First, we found that cilia KOs exhibited drastically reduced EEG waveform activity (Fig. 2H). The EEG amplitude of cilia KOs was much smaller than controls (Fig. 2H). Second, cilia KOs needed much shorter time to be induced by 3% isoflurane to reach the isoelectric (brain-death) stage (Fig. 3I). Moreover, the duration of slow wave oscillation (Fig. 2J), the spike number during slow-wave (frequency < 1 Hz), and bursting numbers (Fig. 2H), and duration of burst suppression (Fig. 2K) under isoflurane-induced anesthesia are drastically decreased in cilia KOs compared to littermate controls (Fig. 2H-K). These data suggest that the general brain activity of cilia KOs is markedly reduced. Due to its severe defects in memory behaviors and EEG brainwaves, this mouse model is very useful in helping evaluate our method to determine primed neurons.

Burst synchronization is a key feature associated with trace fear conditioning memory

We subjected control and cilia KO mice to trace fear conditioning in conjunction with *in vivo* calcium imaging. We monitored the calcium dynamics of the hippocampal neurons during the whole conditioning procedure including training and recall testing, prior to training and prior to recall, as well as under isoflurane-induced anesthesia for normalization. Prior to training, both control's and cilia KO's calcium traces exhibit irregular dynamics (Fig. 3A-B). At training cy1, calcium traces of the control animal started to show some bursts, but the correlation among neurons was very weak. Starting from the 4^{th} training cycle, animal behavior shows a strong difference between control and KO mice and calcium traces from the control animals formed obvious synchronization. The major pattern of all neurons from the control in the 4^{th} training cycle displayed clear bursting, whereas that of cilia KO mouse did not. A strong burst synchronization correlating with animal behavior (freezing bar) was formed among the control neurons at the 7^{th} training cycle. Its major pattern displayed clear bursts responding to tone-on and tone-off (Fig. 3A). After resting for 2 hours, these calcium traces went back to randomly active, similar to that prior to training. Upon recall, they underwent tone-induced synchronization quickly (Fig. 3A). In contrast, cilia KO mouse

cannot form a clear synchronization during training or recall (Fig. 3B). We also constructed time-frequency plots using these calcium traces. Consistently, control neurons exhibit bursting pattern at training cy4 - cy7 as well as during recall testing, whereas cilia KO neurons failed to show bursts.

Next, to examine if neural synchronization is maintained among the same group of neurons, we built heatmaps using pair-wise neural correlation from training to recall testing. All neurons were ranked following the sum of their synchronization levels with the major pattern of PCA (at training cy4, cy7 and a successful recall testing), the same factor used for neuron classification (details explained the next section). These neurons were put at constant position in the heatmaps from training to recall and neurons with higher synchronization values were put on the top. In the control mouse, neurons in the top-left corner were highly synchronized with each other. Pair-wise neural synchronization started to take shape in training cycle 4 and formed a stronger correlation when the mouse was well-trained in cycle 7. Moreover, the pair-wise neural synchronization partially re-emerged during recall testing (Fig. 3C-top). In contrast, cilia KO neurons had much fewer changes in pair-wise neural synchronization during training and recall testing (Fig. 3C-bottom). These data suggest that neuronal synchronization correlates with mouse freezing behaviors of control mice, which is defective in cilia KOs.

One concern is that after hours rest, the neural synchronization during recall is not very strong. To enhance memory formation and achieve a stronger neural synchronization during recall testing, a reinforced trace fear conditioning was applied to the control animals. This group of animals were subject to two rounds of trace fear conditioning prior to recall testing. Indeed, this enhanced training markedly increased the pair-wise neuronal correlation during recall testing (Fig. 3D). Together, these results support the notion that burst synchronization is closely associated with trace fear memory formation and retrieval.

Sorting out primed neurons based on memory-associated synchrony levels

We observed that trace fear conditioning modified the dynamics of high-activity neurons from irregularity to synchronization. This also resulted in changes of the synchronization level distribution (Fig. 4A). In control mice, the synchronization levels of all neurons displayed a relatively linear distribution prior to training, meaning these neurons were evenly distributed on the 1st principal component. After being trained, high-activity neurons synchronized with each other to dominate the major pattern and also increased the synchronization level. In contrast, cilia KOs did not exhibit many changes over training and recall testing and their synchronization levels of all neurons kept relatively linear (Fig. 4A). Fig. 4A also demonstrates that the trace fear conditioning remarkedly increased the percentage of neurons with synchronization level higher than 0.7 in control mice, but not in KO mice.

All individual neurons were classified based on their synchronization levels compared to corresponding major pattern of all neurons. As a rule of thumb, the synchronization levels higher than 0.9 were counted as very highly correlated; the synchronization levels between 0.7 to 0.9 were counted as highly correlated; the synchronization levels between 0.5 to 0.7 were counted as moderately correlated [34]. Here we postulated that high-activity neurons started to show burst synchronization in the middle of training (e.g. cy4) and can last until the end of training (cy7). In recall, tone-induced synchronization is crucial for memory retrieval. Thus, we summarized the synchronization levels in the middle of training (generally the 4th training cycle), after well-trained (generally the 7th training cycle) and successful recall (whichever 1st or 2nd recall testing) of every neuron to be the level for identification. The cut-off was set as: individual neurons with sum of synchronization level higher than 2.0 was defined as primed neurons; others were non-primed neurons, including silent neurons (sum of synchronization level between -1.5 to 1.5) and intermediately active neurons (sum of synchronization level between 1.5 to 2.0). The activity level of these 3 neuronal groups was compared in terms of their variance and their SD-of-SD values to verify this identification (Fig. 4B-C). Interestingly, these primed neurons dominated their corresponding major patterns extracted by PCA analysis when mice were actively engaged in a trace memory (Fig. S2). In contrast, KO mice did not have many primed neurons, and they did not dominate the major pattern associated with trace fear memory (Fig. S2).

Synchronized activity of primed neurons highly correlates with the freezing behaviors of control mice, but not cilia KOs.

To understand how hippocampal neurons collectively engage in trace fear conditioning, we ran a PCA using all neurons collected from control and cilia KO mice to extract the major calcium dynamic patterns of every imaging cycle. These patterns revealed the major bursting responses of all neurons, which were dominated by the group of primed neurons. We compared the correlation level between these major patterns with mouse freezing behaviors. Behavior results were also displayed as moving SD traces, following the same time-window (0.5 s) as calcium SD traces. The representative pattern of moving SD traces for calcium dynamic and mouse behaviors of a control animal exhibited strong coherence responding to tone during trace fear conditioning and recall (Fig. 4D Top). However, the major pattern of cilia KO neurons displayed no bursts or correlation with behaviors (Fig. 4D Bottom). We quantified and compared the correlation levels of mouse behaviors with the corresponding major patterns between control and cilia KO mice. Prior to training, both control and cilia KO mice had only a weak correlation between behavior and the major pattern. Control mice exhibited increasing correlation levels during training or recall testing, whereas cilia KOs had little changes over the training and recall (Fig. 4E).

If our classification of primed neurons is sound, then candidate primed neurons should dominate the correlation with mouse freezing behavior. To test it, we employed PCA to extract the major pattern selectively from the primed neurons' signals. We also extracted the major pattern using SD traces selected from the bottom 50% non-primed neurons. We conducted a correlation analysis between major patterns of primed and non-primed neurons with mouse locomotion behavioral data, respectively. Fig. 4F shows that the correlation between primed neurons' major pattern with animal locomotion markedly increased with training, then returned to the basal level during rest, and increased again upon recall testing, while non-primed neurons did not show such an increase with training or upon recall. Note that we were unable to determine enough primed neurons from each cilia KO mouse to permit PCA to extract any pattern. Together, these data confirm that the synchronized activity of primed neurons highly correlates with the freezing behaviors during the training of controls.

Ift88 cilia KO mice display drastically reduced hippocampal neuronal activity

We converted neuronal calcium traces into 5-second moving SD traces, which reflect the magnitude of the fluctuations of calcium dynamic. A trace with a bursting pattern has significant variation in the SD trace over time. The variation in the SD trace in time can be measured by taking another standard deviation of the entire SD trace. This new quantity, which we name SD-of-SD, gives an indication of the variation in the activity level over the course of the cycle of the experiment (Fig. S1B). We noted that some high-activity neurons tend to form a burst when responding to stimulus or spontaneously when a mouse is trained to engage in trace fear memory [28] (Fig. 1&3). The SD-of-SD, as a measure of "bursting" can be used as alternative method to approximate neural priming. For instance, a neuron that exhibits "bursting", forming a peak when responding to learning cues or spontaneously occurring, followed by a period of low activity, have a high SD-of-SD, while neurons that are either consistently active, consistently inactive, or simply white noise at any amplitude have low values for the SD-of-SD (Fig. S1B). Since the computation of neuronal activity levels was changed from variance to SD-of-SD, the apparent distinctions between primed neurons and intermediately active neurons required a heavier skewed tail, which switched fitting functions from log-normal probability density function to log-logistic probability density function [38]. Fig. S3 presents the differences of log-normal and log-logistic fittings. Apparently, a log-logistic probability density function better fits the SD-of-SD histograms with a prominent long tail, which is filled with imaging data from high-activity neurons (Fig. S3).

We plotted the histograms of the activity levels of individual neurons measured by the SD-of-SD under different conditions (Fig. 5A). Similar to our previous report [28], the neuronal activity histograms are clearly right skewed. Based on the histograms, most neurons having low activity levels were classified as

non-primed neurons, whereas a small portion of neurons with SD-of-SD ratio higher than 3 were considered candidates for primed neurons (Fig. 5A). In control mice, the fitting curves were significantly shifted to right by training, suggesting an increase in activity levels (Fig. 5A-i). It is worth noting that in the right-skewed tail, the number of high-activity neurons was dramatically increased, because of neuronal bursting caused by training. Similar to training, recall testing also led to a clear rightward shift in the neuronal activity levels in control mice (Fig. 5A-ii).

We used cilia KO mice as a negative reference to corroborate our estimation of primed neurons. The activity histograms (measured by SD-of-SD) of cilia KOs are weakly right-skewed, indicating that the number of candidate primed neurons was much fewer in cilia KOs than in control mice. Moreover, trace fear conditioning still caused a rightward shift in the histogram in cilia KOs, but not as strong as controls (Fig. 5A-iii). These data were consistent with impaired memory behaviors (Fig. 2). In recall, neurons in KO mice showed little rightward shift (Fig. 5A-iv). To further compare the activity levels of high-activity neurons that fall into the right-skewed tail, we calculated the cumulative distribution for the SD-of-SD and focused on the top 10% active neurons (Fig. 5B). The extended line from the intersection of each curve and the subline for y = 90% revealed the activity level of top 10% neurons in each group. In control mice, the cut-off for top 10% highly active neurons was increased from 2.22 (prior to training) to 2.98 (when trained) in trace fear conditioning. In cilia KOs, this reduced increase was from 1.49 (prior to training) to 1.63 (trained). Prior to recall, the top 10% cut-off for control mice was 2.0 and increased to 2.38 by the recall cycle. However, cilia KOs exhibited a weaker increase from 1.68 to 1.71 in recall. The violin plots of SD-of-SD in Fig. 5C further confirm a similar result that the neuronal activity levels of control animals shifted dramatically by training and recall, whereas cilia KO neurons have little change.

Since both high neural activity levels and memory-associated burst synchronization are key features of primed neurons, we combined these two factors to make plots of SD-of-SD vs Synchronization to verify the sorting of primed neurons. In Fig. 6, the cut-offs were set as SD-of-SD higher than 3 and the synchronization level higher than 0.7. In control animals, a cluster of primed neurons were sorted out and they appear in the upper-right corner in training cy4 to cy7 and re-appear in recall testing. In contrast, cilia KO animals failed to find many primed neurons in the upper-right corner throughout the training and recall cycles, demonstrating significantly lower number of primed neurons.

Accumulation of non-linear weighting synaptic transmission naturally leads to activity hierarchy in a simulated neural network

To understand how a small fraction of neurons become more active than others (we term it neuronal priming), we developed a simplified computational model consisting of a two-dimensional array of

neurons, in which electrical signals are assumed to propagate from left to right through the array. Each neuron, except in the rightmost column, is assumed to have axon terminals connected to the dendrites of neurons on its right with a variable connection strength S_{ki} (Method, Fig. 7A). Postsynaptic conductance in the brain is mostly mediated by AMPA receptors and NMDA receptors [39], which we simulate as linear and non-linear weighting synaptic transmission components, respectively. The simulation was initialized with each neuron being equivalent (other than starting at random initial activation levels) and every connection of equivalent strength and efficiency. A subset of the left-most neurons was randomly chosen to fire each computational iteration. As signal accumulates and the holding potential depolarizes, neurons in subsequent columns reached the threshold for firing and the iterations were continued to see if primed neurons with high firing rate appear. We found that a moderate ratio of non-linear to linear conductance ratio does produce significant priming patterns and the resulting firing rates show a right-skewed log-logistic distribution (Fig. 7B). Neuronal activity hierarchy naturally developed from left to right, right 10 columns were recruited into firing rate distribution, whereas as the left edge was enforced to be random by the simulation. Fig. 7B right panel presents the firing rate of the entire neuron array during computational iterations, showing that as the impulse signal progressed from left to right, that preferential pathways appear. Fig. 7B left panel shows the histograms of the firing activity level for the last ten layers on the right edge during iterations, demonstrating a significantly right-skewed distribution. The right-skewed log-logistic distribution mimics the neuronal activity distribution measured in our *in vivo* calcium imaging experiments (Fig. 5).

If the priming pattern formation has something to do with the non-linear, the NMDAR gate's opening, then those gates require certain activity levels to open, thus, the low firing activity level will suspension pattern formation. When the patterns do form, the strength of the patterns and speed at which they form is tied to the firing activity level. We also found that basal neuronal activity levels also affect the progression of neuronal priming. We changed the initial basal activity levels in our simulation (from 6% neurons firing in the first layer per cycle to 2% neurons), and we found that no neuronal priming occurs, and the distribution of the firing activity is not significantly skewed nor is there much variation in the firing activity levels (Fig. 7C). Supplemental Video 2 has all the parameters the same as Supplemental Video 1, except the initial activity level on the left side was reduced from 6% to 2%. As Video 2 shows, no neuronal priming patterns emerge over the simulation, while in Supplemental Video 1 (6%), we can start to see the patterns forming by as early as at 5,000 computation iterations, and a very clear right-skewed distribution by 12,500 iterations.

To further correlate our simulation results to the realism of hippocampal memory-eligible neurons, we imaged the expression level of c-Fos that reflects immediate early gene expression in response to 7

cycles of trace fear conditioning. Fig. 7D show that trace fear conditioning significantly increased the c-Fos positive neurons in the CA1 region. Interestingly, we observed that the expression level of c-Fos presents a similar situation that a small portion of cells with very high signal, whereas other neurons had low expression level. We collected more than 1,600 c-Fos positive CA1 neurons out of 5 control mice to construct a histogram. Similar to the right-skewed distribution of calcium dynamics that measured by SD-of-SD, the c-Fos expression levels demonstrated a right-skewed log distribution that can be well fitted by a log-logistic probability density function (Fig. 7E).

Discussion

This report presents multiple critical findings on hippocampal memory-eligible primed neurons: (1) Based on neural activity levels and memory-associated burst synchronization, we have quantitatively determined neuronal activity hierarchy to establish trace memory-eligible "primed" neurons (Fig. 6). (2) PCA of calcium dynamics has revealed that when a trace fear memory is being formed or retrieved, the major pattern of PCA is predominantly mediated by primed neurons and correlated with mouse freezing behaviors. Conversely, when an animal is not actively engaged in mnemonic activity, the major pattern of PCA does not fully distinguish itself from other minor patterns. (3) Cilia KO mice, which exhibit severe learning deficits, have far fewer primed neurons, cannot develop memory-associated burst synchronization, and trace fear conditioning fails to induce a major pattern that is clearly distinguishable from other minor patterns. (4) In our neural network simulation model that incorporates both linear and non-linear weighting synaptic components, primed neurons can naturally develop after 10,000 iterative computations. We found that basal neuronal activity levels also regulate the formation of an activity hierarchy. This simulation suggests that accumulation of non-linear synaptic transmission plays a key role in developing neuronal activity hierarchy.

To better elucidate the cellular and network mechanisms of trace fear memory formation, it is necessary to identify memory-eligible primed neurons and track their real-time dynamics associated with memory acquisition under the physiological condition. However, to date, there is a lack of experimental approaches or numerical methods to determine neural activity hierarchy and quantitatively determine primed neurons that are actively engaged in trace fear conditioning. The previous method relying on c-Fos labeling has limitations. For instance, c-Fos is often pathologically activated by unspecific stimuli such as neuronal injury [40]. Not all c-Fos positive neurons are directly linked to memory formation in some *in vivo* experimental settings, including a two-photon imaging system. It is also noted that c-Fos is expressed 30-60 minutes after neuronal stimulation [3,41,42], reflecting immediate early gene transcription for the cellular-level memory consolidation, however, its expression is transient and does not time-locked

with neural dynamics for memory acquisition. Additionally, while the c-Fos-based engram cell labeling method is widely used in contextual fear memory or spatial memory [5,43,44], its expression dynamics are not well characterized in trace fear conditioning paradigm that requires repetitive training.

Our deep-brain *in vivo* fiber-optic confocal imaging system in conjunction with freely behaving trace fear conditioning avoids GRIN lens implantation injury or pathological neuronal activity, which helps maintain hippocampal neuronal activity very close to the physiological state (Fig. 1). While the imaging system does not yield very clear images of hippocampal neurons, the lateral resolution of the system reaches 3 μm. We have also employed several empirical methods to ensure that ROI data were collected from single cells (Fig. 1I-J). Therefore, this imaging approach is well-suited to determine neuronal activity hierarchy *in vivo*. We combined burst synchronization with the SD-of-SD to establish primed neurons. After eliminating background patterns, we performed a PCA of all imaged neurons to extract a major activity pattern that is associated with fear conditioning and then measure the correlation level of individual neurons with the major pattern. The correlation level of each neuron with the major pattern yields a ranking of hierarchy (Fig. 3-4). We supplemented this method with the SD-of-SD computation (Fig. 5), which clearly differentiates bursting neural activity from low activity and consistent high-amplitude fluctuation and distinguishes primed neurons from non-primed neurons. Nevertheless, it should be noted that the concept of primed neurons, if solely defined by highly active, might be too general. Some active neurons may not be necessarily engaged in a specific type of learning. Including a factor of synchronization and bursting helps refine the scope of primed neurons that actively participate in trace fear memory formation. We used the SD-of-SD that highlights training-induced bursting of primed neurons and found that the SD-of-SD measurement aligns very well with synchronization levels of primed neurons with the major pattern, because primed neurons largely cluster in the upper-right corner in the plot of SD-of-SD vs synchronization levels (Fig. 6). This upper-right cluster becomes pronounced with repetitive training, disappears during rest, and re-appears in a successful recall (Fig. 6). Mouse freezing behaviors correlating with the major pattern of primed neurons also endorses the accuracy of our sorting method (Fig. 5).

Estimation of the percentage of prime neurons. Based on individual neurons' synchronization levels with the major PCA pattern, this study has yielded an estimation of primed neuron percentage in the mouse hippocampus. If the summed value of one neuron at training cy 4, cy7 and a successful recall is more than 2.0, then the neuron is sorted as primed neurons (Fig. 4). We have calculated that the percentage of hippocampal primed neurons is about 9.4 ± 3.4% in control mice (Table 1). This number is very close to other estimations [3,7,45]. It is worth noting that the estimation of primed neuron percentage in the

hippocampus is affected by many variables, such as animal strains and how animals are trained. If mice are repetitively trained for more cycles, more neurons may be counted as primed neurons (Fig. 3D). Indeed, we observed that repetitive training may impact the neural dynamic and priming of hippocampal neurons and recruit more neurons to engage in memory formation. These results also suggest that the pool of primed neurons is not fixed but subject to change. The calculated number of synchronized neurons increases with training cycles, and more neurons remain highly active and synchronized during recall testing (Fig. 4C-D). Conversely, cilia KO mice were found to have lower activity hierarchy and exhibit severe learning deficits. Cilia KOs have drastically reduced neuronal activity and reduced primed neurons with a percentage of 1.9 ± 1.5%. Additionally, cilia KO mice cannot develop much trace memory-associated synchronization, demonstrating the importance of the synchronization among primed neurons in trace memory formation. This also suggests that the decreased number and reduced activity of primed neurons may account for their memory impairment. Cilia KO mice serve as a negative reference in this study to identify primed neurons. The results collected from cilia KO mice is in line with our neural network simulation work, showing that reduced initial neuronal activity affects the development of neural activity hierarchy (Fig. 7). We acknowledge there are many ways to regulate neuronal activity hierarchy. Ablation of primary cilia (Fig. 2) represents just one way out of many that affect the basal neuronal activity in the brain, which consequently modulates the development of neuronal activity hierarchy.

Right-skewed log-normal vs right-skewed log-logistic distributions. We have shown previously that hippocampal neuronal activity levels exhibit a right-skewed log-normal distribution [28]. That measurement was based on the variance of the calcium traces of individual neurons. To highlight hippocampal primed neurons that engaged in trace fear memory and help distinguish primed neurons from non-primed neurons, we have formulated a SD-of-SD method to measure relative neuronal activity. We discovered that before training, the activity histogram of SD-of-SD was well fitted either by a right-skewed log-normal or log-logistic function (Fig. S3). However, when mice are well trained and primed neurons display burst synchronization, the histogram of SD-of-SD starts to have a longer tail on the right. A log-normal function no longer fits, while a log-logistic function, which has an additional degree of freedom, still does. Log-normal and log-logistic distributions are often used for analyzing skewed data [38]. They have similar shapes of their probability density functions in a certain range, but log-logistic distribution can have heavier tails. For the activity histogram having a right-skewed distribution, either of them can be used to fit our data. Here we chose a log-logistic distribution for increasing the weight of right-skewed tail filling with primed neurons during later training cycles (Fig. S3). Our neural network model, which did not include training simulation, revealed the appearance of primed neurons. After 10,000 iterative computations, the neural

firing average can be fitted by a right-skewed log-logistic functions (Fig. 7), which is similar to the right-skewed distribution measured by *in vivo* calcium imaging and the c-Fos expression levels (Fig. 7E).

Why the hippocampus needs to form and maintain a neuronal activity hierarchy? This study, along with many other studies [3,4,6,7], raises an interesting question: why neuronal activity hierarchy is so crucial for hippocampal memory formation or why need the hippocampus form and maintain a neuronal activity hierarchy. There is not much evidence that has addressed such a question. We speculate: (1) An animal does not encounter all sorts of sensory stimuli at one time. Its nervous system may only transduce a small portion of sensory input into the hippocampus for information processing. Thus, only a small portion of hippocampal neurons become active due to limited sensory inputs at a time. (2) There is a high-density of neurons in hippocampal laminae (DG, CA3 and CA1), which facilitate information association. However, it would lead to neuronal over-activation or epilepsy if all neurons in the hippocampus were highly active. (3) If hippocampal neurons were equal in excitability and all were highly active to engage in memory formation, it would cause a huge demand for energy and nutrient support. Glucose or energy supply could not be guaranteed. Glial support such as neurotransmitter synthesis or recycling could not be sufficiently provided. (4) An animal or human acquires new experiences every day, it may need a different cohort of neurons to take turns to encode different memories. (5) Neuronal activity hierarchy may help to encode memory information. Hypothetically, there is some sort of rotational mechanism for hippocampal neurons to become active to participate in hippocampal memory formation. (6) Neuronal activity hierarchy may enable the construction of electrical conduits for information flow and likely build unique neural connectivity in the hippocampus [28]. (7) Neuronal activity hierarchy could facilitate neuronal communication and synaptic plasticity among high-activity primed neurons. Due to increased neuronal excitability, communications between primed neurons are strongly enhanced such that they could coherently develop synchronization. This consequently facilitates activity-dependent synaptic plasticity, critical for memory formation [46-48]. (8) Because of primed neurons and formation of burst synchronization among primed neurons, encoded memory information in the hippocampus could be more easily entrained to the neocortex for the system-level memory consolidation and long-term memory storage in the neocortex. (9) We further speculate that maintaining neuronal activity hierarchy to a certain degree is also crucial for mental health and intellectual ability. Together, neuronal activity hierarchy within a healthy range confers many advantages for information processing and hippocampal memory formation.

One innovation of this study is that we show in our simulation model that non-linear conductance may be crucial the development of neuronal activity hierarchy during iterative synaptic transmission. So far, little is known about the development of neural activity hierarch and the dynamics of neuronal priming,

our neural network simulation study reveals that non-linear synaptic conductance may play a crucial role in the development of neuronal hierarchy. Our simulation data suggest that the NMDAR to AMPAR ratio must be a key factor that impacts the development of neuronal activity hierarchy during iterative computation. In the simulation, if sufficient NMDAR conductance is present, even slight changes in neural activity levels will over time lead to the priming of the most active neurons, while those that have lower activity levels will become relatively silent. Non-linear NMDAR conductance is well known to mediate some forms of hippocampal synaptic plasticity[49,50]. Why is the non-linear, NMDAR conductance so important? This is because of the magnesium-blockade of NMDA receptors. The voltage-dependency of NMDAR [31]makes its current-voltage response non-linear, the more active a neuron is, the more easily it sheds the magnesium blockade to allow even stronger NMDAR conductance, resulting in an intensifying effect [51].

Limitations of this study: (1) Limitations of the experimental system. (i) This study did not employ an engram cell labeling technique [52,53] to selectively label memory-eligible neurons, thereby this work cannot directly link what have identified "primed neurons" to c-Fos positive cells. To validate the quantification of neuronal activity hierarchy or the identity of primed neurons, future experiments will require the use of chemogenetic or optogenetic tools in conjunction with engram cell labeling technique to manipulate memory-eligible cells. (ii) Another limitation of the fiber-optic imaging approach is its low imaging sensitivity. This imaging approach can detect strong calcium influx into a neuron, but cannot distinguish weak calcium entry or resolve individual calcium spikes. The fiber-optic imaging system converts weak calcium signals into basal fluctuation. High fluctuation or strong bursting indicates high neuronal activity, while flat calcium trace denotes low neuronal activity (not necessarily completely silent). Therefore, this limitation does not prevent us from determining activity hierarchy. (iii) This study we have only used mouse trace fear conditioning as a behavioral paradigm to quantify neuronal activity hierarchy. The conclusion may be biased by trace fear conditioning, which is a temporal aversive memory association. Other types of memory-related behavioral paradigms should be employed in future studies to test the generality of this method.

Our neural network model simulates neural communication and neural priming seemingly consistent with our experimental results. However, the model does not fully account for exact processes for AMPAR, NMDAR, and voltage-gated ion channels that mediate synaptic transmission and action potential. Another limitation in the model is that it is a fast-scale algorithm and does not incorporate slow-scale effects such as neural plasticity and that after significant activity primed neurons will rest. By not letting active primed neurons rest, continuing well past 12,500 iteration, with the parameters used in our

study, can lead to a slight bifurcation in neural activity will too many heavily primed neurons and fewer intermediate. It is believed that an appropriate algorithm for resting long active neurons is implemented in the simulation, histograms such as those obtained at 12,500 iterations will be maintained indefinitely. Implemented and testing this hypothesis is part of our future work. While some parameters that would be needed for a precise model are, as yet, unknown, and some aspects of the model, such as the neural connectivity structure could never precisely imitate nature, future simulation work will further evolve this model to: (i) increase its realism by incorporating equations for ion channels; (ii) further test effects of other factors on the development of primed neurons and thereby refine the theories; (iii) introduce greater generality in the simulation to better understand other regulatory processes behind neural communication; (iv) include a factor of training to model the development of burst synchronization of primed neurons.

In summary, we report a novel method to measure neuronal activity hierarchy and sort out trace fear memory-eligible primed neurons. We found that cilia KO mice have a reduced percentage of primed neurons and exhibit severe learning deficits. Our simulation work further revealed that accumulation of non-linear synaptic transmission, likely mediated by NMDAR-mediated conductance, may explain how a small group of hippocampal neurons are primed to preferentially engage in memory formation. Determination of neuronal activity hierarchy in the hippocampus and elucidating the mechanisms of neuronal priming will help understand how neurons are selectively recruited and interact within the network to encode and store hippocampal memories. Additionally, it will guide future experiments to manipulate these memory-eligible primed neurons to reveal their emergence and disappearance dynamics.

Table 1: Comparisons of primed neurons with non-primed neurons

		Primed Neurons	Non-Primed Neurons	
			Intermediate	Silent
Variance of calcium traces	Prior to training (basal)	High	High	Low
	Trained	Higher	High	Low
	Recall testing	High	High	Low
SD of 5s-SD traces (SD-of-SD)	Prior to training (basal)	High	Mid	Low
	Trained	Higher	Mid	Low
	Recall testing	High	Low	Low
Position in right-skewed log distribution		Right tail	between	Middle & left
Form significant burst synchronization during conditioning?		Yes	Weak	No
Form significant burst synchronization during recall?		Yes	Weak	No
Synchronization level with 1st PCA component		High	Middle	Low
Correlation with mouse freezing behavior during training		Yes	Weakly	No
Correlation with mouse freezing behavior during recall testing		Yes	No	No
Calcium burst responding to tone or foot shock when trained		Strong	weak	No
Engage in trace memory formation and retrieval?		Highly engaged	Weakly or not engaged	
Percentage in control mice		9.4% ± 3.4%	16.8% ± 9.2%	73.7% ± 11.8%
Percentage in cilia KO mice (low hierarchy)		1.9% ± 1.5%	6.4% ± 2.9%	91.7% ± 4.3%

Figure Legends:

Fig. 1. Minimally invasive surgery and one-day imaging at the cellular resolution avoids hippocampal inflammation and pathological neuronal activation. (A) Top: Illustration of the surgical setup where the imaging window (d = 0.8 mm) aligned with an imaging cannula, which were stabilized by screws and dental cement. Bottom: A cross-section of the surgical setup. Cannula implantation surgery was installed above the skull and surgery only slightly affected the surface of neocortex and did not the hippocampus. **(B)** Immunofluorescence staining using c-Fos antibody on hippocampal slices 8 weeks after AAV-Syn-GCaMP6m injection and canula stereotaxic surgery but right before *in vivo* fiber-optic imaging. Left: non-surgical hemisphere showing c-Fos positive neurons. Right: surgical side from same brain slice with GCaMP6m expression (green), showing similar levels of c-Fos expression (magenta). **(C)** GFAP staining (an indicator for reactive astrogliosis) shows no differences between the surgical and non-surgical hemispheres. **(D-E)** Statistics of c-Fos-positive neuron number **(D)** and GFAP fluorescence intensity **(E)** relative to DAPI in non-surgical and surgical hemispheres. There was no difference between non-surgical and surgical hemispheres, paired Student T-test. **(F)** Three days after imaging, imaged hippocampal tissues (right) displayed signs of astrogliosis, as evidenced by heightened expression of GFAP. The left non-imaged hemisphere had no signs of gliosis. **(G)** A mouse carrying an imaging probe could behave freely. **(H)** A whole view of endoscopic image. 3 distantly located areas (white boxes) were selected and enlarged in **(I)** to demonstrate the single cell resolution of imaging. **(I)** In each area, one primed neuron (red ROI and red trace) was surrounded by several non-primed neurons (grey ROIs and grey traces). Green traces were calcium signals collected from one fiber located at the center of primed neurons. One-fiber signals (green ROIs and green traces) had a lower signal-to-noise ratio, but their dynamics were very similar to multiple fibers signals (red traces) that covered a larger area. Primed neurons were randomly active prior to training but developed a bursting pattern when the mouse was trained and engaged in conditioning. These separately distributed primed neurons (red) also synchronized with each other (i, ii and iii), whereas neighboring non-primed neurons (grey) showed little bursting patterns or synchronization after being trained. **(J)** An empirical method to identify single cell ROIs. An 8-fiber ROI covering a large area and more than one neuron (golden). Individual fibers are shown in the left image. Calcium traces of each fiber (#1-8) are shown in the right, which can be classified into two groups (A and B). Neuron A encompasses fiber 1-4 (all showing similar calcium dynamics), while neuron B contains fiber 5-8 (all showing another pattern). Thus, the 8-fiber ROI was interpreted to cover 2 neurons (A and B). **(K)** A scheme showing the procedure of imaging data pre-processing and subsequent data analysis.

Fig. 2. Ift88 cilia KO mice exhibit severe learning deficits in trace fear conditioning tests and Morris water maze, and decreased EEG activity under anesthesia. (A) Immunofluorescence staining using AC3 antibody on hippocampal slices. 8 weeks after tamoxifen administration to induce cilia ablation in Ift88 cilia KOs. Top: The hippocampus of control animal has cilia; Bottom: KO mice showed absence of cilia. **(B)** Trace fear conditioning test. Freezing scores of mice (moving speed < 0.1 cm/s) in trace periods during training. n = 10 pairs, mixed sexes. Cilia KO mice exhibited severe learning deficit and their freezing scores are much lower than controls. Bonferroni's multiple comparisons test of two-way ANOVA, controls vs KO mice. **(C)** Mouse freezing scores ratio between 10 mins after and 10 mins prior to training. Control mice had a significantly higher ratio than cilia KOs, unpaired Student T-test. **(D)** Freezing scores of mice in recall. Control mice exhibited significantly higher tone-induced freezing than cilia KOs in 2nd recall cycle, Bonferroni's multiple comparisons test of two-way ANOVA, controls vs KOs. **(E-G)** Morris water maze test. Cilia KO mice exhibit spatial memory in Morris water maze test. n = 10 pairs, mixed sexes. **(E)** Control mice learned quicker in the training part of Morris water maze. Repeated measure one-way with post hoc Tukey's multiple comparisons test between training day1 and every other day. Bonferroni's multiple comparisons test of two-way ANOVA, controls vs KO mice (above X-axis). **(F)** Representative Morris water maze probe test of control and cilia KO mice. **(G)** Morris water maze probe test: cumulative durations of control and cilia KO mice in each quadrant. Control mice spent a significantly longer time in the target quadrant than the other 3 quadrants whereas cilia KOs revealed no difference. Repeated measure one-way with post hoc Tukey's multiple comparisons test between target quadrant and other 3 quadrants. **(H-K)** Cilia KOs need much less time than controls to be fully anesthetized and reach the isoelectric stage (brain death). **(H)** EEG recording monitoring brain waveform during isoflurane-induced anesthesia. 3% isoflurane (ISO) was used to induce anesthesia. Left: Control; Right: cilia KO. EEG traces at different anesthesia stages are enlarged below. (i), before ISO (awake); (ii-iii), slow wave oscillation and burst suppression (BS) period; (iv), the isoelectric brain-death stage. Quantification of the time to reach the isoelectric (brain death) stage **(I)**, duration of slow oscillation **(J)**, and duration of burst suppression **(K)**. Anesthetic EEG data were collected from 12 control mice and 9 cilia KO mice (mixed sexes). Unpaired Student T-test between control and cilia KO mice. ns, not significant; *, $p<0.05$; **, $p<0.01$; ***, $p<0.001$.

Fig. 3. Primed hippocampal neurons of control mice, not cilia KO mice, develop memory-associated burst synchronization. (A) (Top**)** Representative traces of 7 high-activity neurons from a control mouse. White bars: mouse moving; black bars: freezing. (Middle) The major patterns (1st principal component of PCA) extracted from all individual neurons out of the same animal. (Bottom) Time-frequency plots of

calcium dynamics of 7 high-activity neurons. **(B)** (Top) Representative traces of 7 high-activity neurons from one cilia KO mouse. (Middle) The major patterns (1st principal component of PCA) extracted from all individual neurons out of the same KO mouse. (Bottom) Time-frequency plots of calcium dynamics. High-activity neurons of control mice can form burst synchronization in late training cycles or early recall testing, whereas those of cilia KO mice don't display bursts or a specific pattern. **(C)** Heatmap of correlation levels between every two neurons from a control mouse (top) and a KO mouse (bottom) same as (A-B). The same neuron was placed at the same position in these heatmaps. In the control mouse, the same group of neurons displays high correlation levels during both training and recall testing, whereas neurons in the cilia KO mouse have weak synchronization and no clear pattern. **(D)** Enhanced training promotes neuronal synchronization during recall in controls. Reinforced trace fear conditioning paradigm: 7 cycle training (not imaged) - 2 hours rest - 7 cycle training again (imaged) - 3 hours rest - recall (imaged). Pairwise neuron synchronization levels are indicated warm color.

Fig. 4. Sorting out primed neurons; synchronization of primed neurons is correlated with trace fear conditioning in control mice, but not in cilia KO mice. (A) Synchronization level distribution of two controls and two cilia KO mice at different training or recall conditions. Synchronization level distribution in control animals increases with training and recall testing, whereas those of KO animals have little change with training and recall. **(B-C)** Bar graph of neuronal activity levels of three groups of neurons under different conditions. The variance (B) and SD-of-SD (C) of raw calcium dynamics. SD-of-SD for individual neurons allowed for distinguishing the primed neurons from the intermediate neuron group at later training cycles (Fig. 2B). Data were collected from ~500 neurons from 5 control animals. Ordinary one-way ANOVA with post-hoc Tukey's multiple comparison. **(D)** Top: 0.5s-moving SD trace of all neurons major pattern (orange) and freezing behavior (black) of one control mouse. The control animal had a clear response to tone and shock when trained. Moreover, the major pattern showed a response to stimulus and a strong correlation with behavior. Bottom: 0.5s-moving SD trace of all neurons major pattern and freezing behavior from one cilia KO mouse. The major pattern of this cilia KO animal cannot develop an obvious burst. **(E)** Correlation between neurons' major pattern and behavior data (n = 5 pairs, mixed genders). The correlation levels of control animals were increased by training and recall. The correlation levels of cilia KO mice showed no difference over training and recall testing. Repeated measure one-way ANOVA with post hoc Tukey's multiple comparisons test between prior to training and each other cycle. Paired Student T-test between prior to recall and successful recall. **(F)** Correlation between primed neurons' and bottom 50% neurons' major patterns and behavior data in control animals (n = 5, mixed genders). The correlation levels of primed neurons were significantly higher than the bottom

50% neurons in training and successful recall. Bonferroni's multiple comparisons test of two-way ANOVA, primed neurons vs bottom 50% neurons. ns, not significant; *, p<0.05; **, p<0.01; ***, p<0.001.

Fig. 5. Reduced hippocampal neuronal activity in Ift88 cilia KO mice. (A) Activity histograms of individual neurons in control mice (left, green) and cilia KO mice (right, red). The SD-of-SD for individual neurons prior to training (top, dashed), at training cycle 7 (cy7) (top, solid), prior to recall (bottom, dashed), and during recall (bottom, solid) normalized to those under anesthesia. The fitting curves fitted log-logistic distribution; the K-S test was used to compare the difference. Control: n = 506 neurons from 5 control animals. K-S test between Prior to training and the end of training, ***, p < 0.001; prior to recall vs successful recall, ***, p < 0.001. Cilia KOs: n = 541 neurons. K-S test between prior to training and the end of training, **, p = 0.004; prior to recall vs successful recall, ns, p = 0.13. **(B)** Cumulative distribution of the activity level of individual neurons in controls (green) and cilia KOs (red). The guides were set on y = 90% to highlight the neurons having the top 10% of activity levels. The extended lines labeled the intersections between every curve and the guides. The highlighted boxes were zoomed in at the bottom. **(C)** Violin plots of SD-of-SD of calcium dynamics at different training cycles. Left, controls; Right, cilia KOs. Data were collected from 506 neurons out of 5 control animals and 541 neurons out of 5 cilia KO animals. The SD-of-SD shows a rightward shift over training or upon recall in control animals, but not in cilia KOs.

Fig. 6. Plotting synchronization levels against SD-of-SD to identify primed neurons. Plots of the synchronization (to the major pattern) vs the activity level of individual neurons. Controls (left) and cilia KO mice (right). X-axis is the SD-of-SD of individual neurons normalized to the basal level of isoflurane-induced anesthesia, Z-scored. Y-axis is the synchronization level of individual neurons compared to the major pattern of PCA. Dashed lines at Y = 0.7: neurons with synchronization levels higher than 0.7 were consider high synchronization; Dashed lines at X = 3: neurons with activity levels (SD-of-SD) higher than 3 were viewed as high activity. Neurons in the top-right (with high synchronization and high activity) were defined as primed neurons. Based on the combined calculation from cy4, cy7, and a successful recall, control mice have markedly more primed neurons than cilia KO.

Fig. 7. Accumulation of non-linear weighting synaptic transmission naturally leads to activity hierarchy in a simulated neural network. (A) Neural network simulation. A fired pre-connected neuron (N_{ij} at row i, column j) releases neural transmitters from pre-synapse, the post-synaptic conductance of the next layer neuron ($N_{k(j+1)}$) mostly mediated by AMPA receptor (linear component) and NMDA receptors

(nonlinear component). The connection strength S_{ki} is dependent on the distance between neurons. The efficiency of NMDAR is dependent on the opening rate of NMDA gate which are affected by post-synaptic activity. **(B)** Firing rate for the entire simulation after 7,500, 10,000 and 12,500 computation iterations, showing pattern development and neural priming resulting in the amplification as signal travels toward the right of random differences in activity levels on the left (right). Firing average observed in the right-most ten columns of neurons in the simulation with moderate NMDAR to AMPAR expression ratio (27.5% NMDAR and 72.5% AMPAR) after different computational iterations. Left: The histogram contributed by the firing rate of neurons in right-most ten columns after different computing iterations. Activity histograms are similar in appearance to those that have been measured in calcium imaging or c-Fos expression (E). **(C)** same as **(B)** with reduced initial basal activity levels. Reduced initial neuronal activity does not lead to neuronal priming. **(D)** c-Fos expression in the hippocampal CA1. (Top) Naïve, mice were not subject to tone or foot shock stimulation; (Bottom) Trained, c-Fos expression 30 min after mice were subject to 7 cycles of trace fear conditioning. **(E)** Histogram of c-Fos expression (normalized to the c-Fos intensity average) in the CA1 45 min after trace fear conditioning. It shows a right-skewed log-distribution and is well fitted with a log-logistic function.

Supplemental Figure Legends:

Fig. S1. Imaging data pre-processing and background pattern elimination. (A) A raw calcium trace was transformed into 5-second moving SD trace. A 5-second time-window was moving over the image trace frame by frame and computed the SD to generate a 5s-moving SD trace. **(B)** Representative raw calcium image traces (left) and 5s-moving SD traces (right) of high-activity neurons (warm colors), 4 intermediate active neurons (cold colors), and 4 silent neurons (grey). Prior to training (Left) and trained (Right). SD-of-SD of calcium dynamics helps distinguish primed neurons. **(C)** The Cellvizio confocal fluorescence endoscopic system contains ~7600 optic-fibers to detect and average temporal GCaMP6m calcium signals of neurons (images in dashed box having different contrast setting). 12 background ROIs (grey) were defined as a circle covering 50 fibers with minimum GcaMP6 signals to collect background imaging information, which were served as references to eliminate potential motion artifacts or background noise patterns. PCA of 12 background ROIs generated principal components for background subtraction. The SD traces are each normalized prior to the PCA. Principal components with PCA levels above the average were used for background noise elimination. **(D)** Representative fluorescence imaging traces of 7 primed neurons (color) and 2 non-primed (grey) neurons were selected. **(E)** Representative time-stamped images of 3 primed neurons (#1-3) and 1 non-primed neurons (#4). Black arrows denote the 3 time-points when images were acquired. **(F)** Neuronal images were first transformed into 5s-moving SD

traces. The major background patterns were then used to subtract motion artifacts or background noise stepwise. The arrows label the artifacts which identified and removed after background elimination. Afterwards, a PCA analysis was performed based on signals after background removed. The major pattern obtained from the subsequent PCA is shown on the bottom. The correlation levels of the SD traces of all individual neurons to the major pattern were computed to obtain the synchronization level for identifying primed neurons.

Fig. S2. The major pattern of PCA of calcium dynamics is mostly mediated by primed neurons when animals are actively engaged in trace fear memory. PCA of neural calcium dynamics from controls and cilia KO mice. Data points are individual neurons' synchronization level with the principal components (1^{st} and 2^{nd}). The X-axis is the 1^{st} principal component which explains the major pattern. Y-axis is the 2^{nd} principal component after extracting the 1^{st} component. Arrows pointing from zero to the mean center show the vector addition of two components. In control animals (left), training and recall testing increased the weight of the 1^{st} principal component. Individual data points moved to the right, favoring the 1^{st} principal component, while the 2^{nd} principal component remained equally distributed. This change was largely led by primed neurons (labeled in red). In cilia KO animals (right), individual data points were equally distributed on 1^{st} and 2^{nd} principal components and training and recall testing did not cause marked changes. Data were collected from 506 neurons out of 5 control mice and 541 neurons out of 5 cilia KO mice (mixed sexes).

Fig. S3. (A) Neuronal activity levels measured by SD-of-SD of calcium traces. The histograms of right-skewed distribution of SD-of-SD of individual neurons at different training cycles are shown. Solid curves were fitted with a log-logistic probability density function; dashed curves were fitted with a log-normal probability density function. **(B)** Neuronal activity levels measured by variance of calcium traces. The histograms of right-skewed distribution of variance at different cycles are shown. P values of those fitting are shown. Log-logistic probability density function fits these histograms better than lognormal.

Supplemental Video 1: Normal initial neuronal activity naturally leads to the appearance of primed neurons over 12,500 computation iterations.

Supplemental Video 2: Lower initial neuronal activity does not lead to the emergence of primed neurons over 12,500 computation iterations.

Reference:

1 Semon, R. The Mneme. *G. Allen & Unwin* (1921).

2 Hebb, D. O. The Organization of behavior: a neuropsychological theory. *Wiley, New York, NY* (1949).

3 Reijmers, L. G., Perkins, B. L., Matsuo, N. & Mayford, M. Localization of a stable neural correlate of associative memory. *Science* **317**, 1230-1233, doi:10.1126/science.1143839 (2007).

4 Tonegawa, S., Pignatelli, M., Roy, D. S. & Ryan, T. J. Memory engram storage and retrieval. *Current opinion in neurobiology* **35**, 101-109, doi:10.1016/j.conb.2015.07.009 (2015).

5 Josselyn, S. A., Kohler, S. & Frankland, P. W. Finding the engram. *Nature reviews. Neuroscience* **16**, 521-534, doi:10.1038/nrn4000 (2015).

6 Tonegawa, S., Liu, X., Ramirez, S. & Redondo, R. Memory Engram Cells Have Come of Age. *Neuron* **87**, 918-931, doi:10.1016/j.neuron.2015.08.002 (2015).

7 Tonegawa, S., Morrissey, M. D. & Kitamura, T. The role of engram cells in the systems consolidation of memory. *Nature reviews. Neuroscience* **19**, 485-498, doi:10.1038/s41583-018-0031-2 (2018).

8 Semon, R. Die Mneme als erhaltendes Prinzip im Wechsel des organischen Geschehens. *(Leipzig: Wilhelm Engelmann)* (1904).

9 Schacter, D. L. Constructive memory: past and future. *Dialogues in clinical neuroscience* **14**, 7-18 (2012).

10 Josselyn, S. A. & Tonegawa, S. Memory engrams: Recalling the past and imagining the future. *Science* **367**, doi:10.1126/science.aaw4325 (2020).

11 Ramirez, S. *et al.* Activating positive memory engrams suppresses depression-like behaviour. *Nature* **522**, 335-339, doi:10.1038/nature14514 (2015).

12 Ramirez, S. *et al.* Creating a false memory in the hippocampus. *Science* **341**, 387-391, doi:10.1126/science.1239073 (2013).

13 Liu, X. *et al.* Optogenetic stimulation of a hippocampal engram activates fear memory recall. *Nature* **484**, 381-385, doi:10.1038/nature11028 (2012).

14 Tayler, K. K., Tanaka, K. Z., Reijmers, L. G. & Wiltgen, B. J. Reactivation of neural ensembles during the retrieval of recent and remote memory. *Current biology : CB* **23**, 99-106, doi:10.1016/j.cub.2012.11.019 (2013).

15 Pignatelli, M. *et al.* Engram Cell Excitability State Determines the Efficacy of Memory Retrieval. *Neuron* **101**, 274-284 e275, doi:10.1016/j.neuron.2018.11.029 (2019).

16 Khalaf, O. *et al.* Reactivation of recall-induced neurons contributes to remote fear memory attenuation. *Science* **360**, 1239-1242, doi:10.1126/science.aas9875 (2018).

17 Roy, D. S. *et al.* Distinct Neural Circuits for the Formation and Retrieval of Episodic Memories. *Cell* **170**, 1000-1012 e1019, doi:10.1016/j.cell.2017.07.013 (2017).

18 Kitamura, T. *et al.* Engrams and circuits crucial for systems consolidation of a memory. *Science* **356**, 73-78, doi:10.1126/science.aam6808 (2017).

19 Han, J. H. *et al.* Neuronal competition and selection during memory formation. *Science* **316**, 457-460, doi:10.1126/science.1139438 (2007).

20 Zhou, Y. *et al.* CREB regulates excitability and the allocation of memory to subsets of neurons in the amygdala. *Nat Neurosci* **12**, 1438-1443, doi:10.1038/nn.2405 (2009).

21 Yiu, A. P. *et al.* Neurons are recruited to a memory trace based on relative neuronal excitability immediately before training. *Neuron* **83**, 722-735, doi:10.1016/j.neuron.2014.07.017 (2014).

22 Frankland, P. W. & Josselyn, S. A. Memory allocation. *Neuropsychopharmacology : official publication of the American College of Neuropsychopharmacology* **40**, 243, doi:10.1038/npp.2014.234 (2015).

23 Kim, J., Kwon, J. T., Kim, H. S., Josselyn, S. A. & Han, J. H. Memory recall and modifications by activating neurons with elevated CREB. *Nat Neurosci* **17**, 65-72, doi:10.1038/nn.3592 (2014).
24 Park, S. *et al.* Neuronal Allocation to a Hippocampal Engram. *Neuropsychopharmacology : official publication of the American College of Neuropsychopharmacology* **41**, 2987-2993, doi:10.1038/npp.2016.73 (2016).
25 Rashid, A. J. *et al.* Competition between engrams influences fear memory formation and recall. *Science* **353**, 383-387, doi:10.1126/science.aaf0594 (2016).
26 Cai, D. J. *et al.* A shared neural ensemble links distinct contextual memories encoded close in time. *Nature* **534**, 115-118, doi:10.1038/nature17955 (2016).
27 Ghandour, K. *et al.* Orchestrated ensemble activities constitute a hippocampal memory engram. *Nature communications* **10**, 2637, doi:10.1038/s41467-019-10683-2 (2019).
28 Zhou, Y., Qiu, L., Wang, H. & Chen, X. Induction of activity synchronization among primed hippocampal neurons out of random dynamics is key for trace memory formation and retrieval. *FASEB J* **34**, 3658-3676, doi:10.1096/fj.201902274R (2020).
29 Mori, H. & Mishina, M. Structure and function of the NMDA receptor channel. *Neuropharmacology* **34**, 1219-1237, doi:10.1016/0028-3908(95)00109-j (1995).
30 Nowak, L., Bregestovski, P., Ascher, P., Herbet, A. & Prochiantz, A. Magnesium gates glutamate-activated channels in mouse central neurones. *Nature* **307**, 462-465, doi:10.1038/307462a0 (1984).
31 MacDonald, J. F. & Nowak, L. M. Mechanisms of blockade of excitatory amino acid receptor channels. *Trends in pharmacological sciences* **11**, 167-172, doi:10.1016/0165-6147(90)90070-O (1990).
32 Haycraft, C. J. *et al.* Intraflagellar transport is essential for endochondral bone formation. *Development* **134**, 307-316, doi:10.1242/dev.02732 (2007).
33 Zhou, Y. *et al.* Comparative Phosphoproteomic Profiling of Type III Adenylyl Cyclase Knockout and Control, Male, and Female Mice. *Front Cell Neurosci* **13**, 34, doi:10.3389/fncel.2019.00034 (2019).
34 Mukaka, M. M. Statistics corner: A guide to appropriate use of correlation coefficient in medical research. *Malawi Med J* **24**, 69-71 (2012).
35 Schindelin, J. *et al.* Fiji: an open-source platform for biological-image analysis. *Nat Methods* **9**, 676-682, doi:10.1038/nmeth.2019 (2012).
36 Chen, X. *et al.* Ablation of Type III Adenylyl Cyclase in Mice Causes Reduced Neuronal Activity, Altered Sleep Pattern, and Depression-like Phenotypes. *Biol Psychiatry* **80**, 836-848, doi:10.1016/j.biopsych.2015.12.012 (2016).
37 Bowie, E. & Goetz, S. C. TTBK2 and primary cilia are essential for the connectivity and survival of cerebellar Purkinje neurons. *Elife* **9**, doi:10.7554/eLife.51166 (2020).
38 Dey, A. K. & Kundu, D. Discriminating Between the Log-Normal and Log-Logistic Distributions. *Communications in Statistics - Theory and Methods* **39**, 280-292, doi:10.1080/03610920902737100 (2009).
39 Kessey, K. & Mogul, D. J. NMDA-Independent LTP by adenosine A2 receptor-mediated postsynaptic AMPA potentiation in hippocampus. *J Neurophysiol* **78**, 1965-1972, doi:10.1152/jn.1997.78.4.1965 (1997).
40 Bullitt, E. Expression of c-fos-like protein as a marker for neuronal activity following noxious stimulation in the rat. *J Comp Neurol* **296**, 517-530, doi:10.1002/cne.902960402 (1990).
41 Sharp, F. R., Sagar, S. M., Hicks, K., Lowenstein, D. & Hisanaga, K. c-fos mRNA, Fos, and Fos-related antigen induction by hypertonic saline and stress. *J Neurosci* **11**, 2321-2331, doi:10.1523/JNEUROSCI.11-08-02321.1991 (1991).
42 Sheng, M. & Greenberg, M. E. The regulation and function of c-fos and other immediate early genes in the nervous system. *Neuron* **4**, 477-485, doi:10.1016/0896-6273(90)90106-p (1990).

43 Miyashita, T., Kikuchi, E., Horiuchi, J. & Saitoe, M. Long-Term Memory Engram Cells Are Established by c-Fos/CREB Transcriptional Cycling. *Cell Rep* **25**, 2716-2728 e2713, doi:10.1016/j.celrep.2018.11.022 (2018).

44 Guzowski, J. F., Setlow, B., Wagner, E. K. & McGaugh, J. L. Experience-dependent gene expression in the rat hippocampus after spatial learning: a comparison of the immediate-early genes Arc, c-fos, and zif268. *J Neurosci* **21**, 5089-5098, doi:10.1523/JNEUROSCI.21-14-05089.2001 (2001).

45 Rubin, A., Geva, N., Sheintuch, L. & Ziv, Y. Hippocampal ensemble dynamics timestamp events in long-term memory. *Elife* **4**, doi:10.7554/eLife.12247 (2015).

46 Martin, S. J., Grimwood, P. D. & Morris, R. G. Synaptic plasticity and memory: an evaluation of the hypothesis. *Annu Rev Neurosci* **23**, 649-711, doi:10.1146/annurev.neuro.23.1.649 (2000).

47 Chaudhury, S., Sharma, V., Kumar, V., Nag, T. C. & Wadhwa, S. Activity-dependent synaptic plasticity modulates the critical phase of brain development. *Brain Dev* **38**, 355-363, doi:10.1016/j.braindev.2015.10.008 (2016).

48 Jeong, Y. *et al.* Synaptic plasticity-dependent competition rule influences memory formation. *Nature communications* **12**, 3915, doi:10.1038/s41467-021-24269-4 (2021).

49 Luscher, C. & Malenka, R. C. NMDA receptor-dependent long-term potentiation and long-term depression (LTP/LTD). *Cold Spring Harbor perspectives in biology* **4**, doi:10.1101/cshperspect.a005710 (2012).

50 Malenka, R. C. & Nicoll, R. A. NMDA-receptor-dependent synaptic plasticity: multiple forms and mechanisms. *Trends in neurosciences* **16**, 521-527, doi:10.1016/0166-2236(93)90197-t (1993).

51 Ge, L. & Liu, X. D. Electrical resonance with voltage-gated ion channels: perspectives from biophysical mechanisms and neural electrophysiology. *Acta Pharmacol Sin* **37**, 67-74, doi:10.1038/aps.2015.140 (2016).

52 Mayford, M. The search for a hippocampal engram. *Philosophical transactions of the Royal Society of London. Series B, Biological sciences* **369**, 20130161, doi:10.1098/rstb.2013.0161 (2014).

53 Liu, X., Ramirez, S., Redondo, R. L. & Tonegawa, S. Identification and Manipulation of Memory Engram Cells. *Cold Spring Harbor symposia on quantitative biology* **79**, 59-65, doi:10.1101/sqb.2014.79.024901 (2014).

Fig. 1

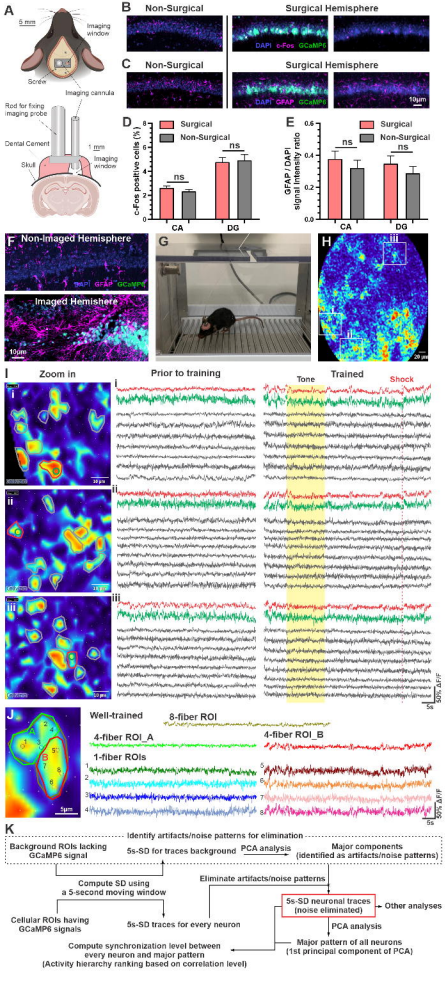
A
5 mm
Imaging window
Screw
Imaging cannula
Rod for fixing imaging probe
Dental Cement
1 mm
Skull
Imaging window
B
Non-Surgical
Surgical Hemisphere
DAPI c-Fos GCaMP6
C
Non-Surgical
Surgical Hemisphere
10μm
DAPI GFAP GCaMP6
D
Surgical
Non-Surgical
c-Fos positive cells (%)
ns
ns
CA
DG
E
Surgical
Non-Surgical
GFAP / DAPI signal Intensity ratio
ns
ns
CA
DG
F
Non-Imaged Hemisphere
DAPI GFAP GCaMP6
Imaged Hemisphere
10μm
G
H
i
ii
iii
2 mm
I
Zoom in
Prior to training
Trained
Tone
Shock
i
ii
iii
50 μm
50% ΔF/F
5s
J
Well-trained
8-fiber ROI
4-fiber ROI_A
4-fiber ROI_B
1-fiber ROIs
5μm
50% ΔF/F
5s
K
Identify artifacts/noise patterns for elimination
Background ROIs lacking GCaMP6 signal
5s-SD for traces backgroung
PCA analysis
Major components (identified as artifacts/noise patterns)
Compute SD using a 5-second moving window
Eliminate artifacts/noise patterns
5s-SD neuronal traces (noise eliminated)
Other analyses
Cellular ROIs having GCaMP6 signals
5s-SD traces for every neuron
PCA analysis
Major pattern of all neurons (1st principal component of PCA)
Compute synchronization level between every neuron and major pattern (Activity hierarchy ranking based on correlation level)

Fig. 2

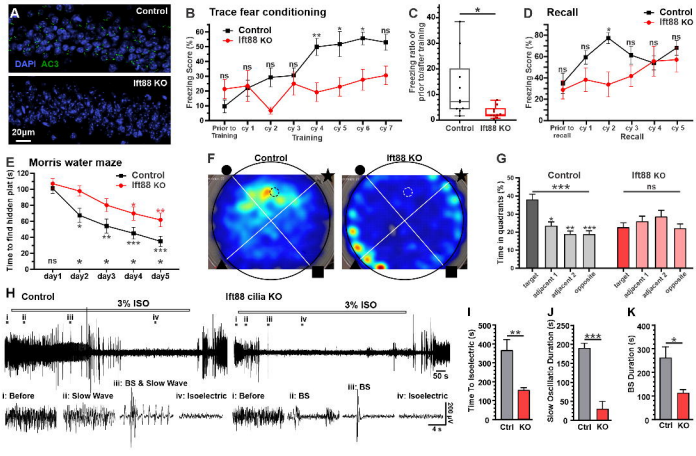
A
Control
DAPI AC3
Ift88 KO
20µm
B
Trace fear conditioning
Control
Ift88 KO
Freezing Score (%)
Prior to Training
cy 1
cy 2
cy 3
cy 4
cy 5
cy 6
cy 7
Training
C
Freezing ratio of prior to after training
Control
Ift88 KO
D
Recall
Control
Ift88 KO
Freezing Score (%)
Prior to recall
cy 1
cy 2
cy 3
cy 4
cy 5
Recall
E
Morris water maze
Control
Ift88 KO
Time to find hidden plat (s)
day1
day2
day3
day4
day5
F
Control
Ift88 KO
G
Control
Ift88 KO
Time in quadrants (%)
target
adjacent 1
adjacent 2
opposite
H
Control
3% ISO
Ift88 cilia KO
3% ISO
50 s
i: Before
ii: Slow Wave
iii: BS & Slow Wave
iv: Isoelectric
i: Before
ii: BS
iii: BS
iv: Isoelectric
200 µV
4 s
I
Time To Isoelectric (s)
Ctrl
KO
J
Slow Oscillatic Duration (s)
Ctrl
KO
K
BS Duration (s)
Ctrl
KO

Fig. 3

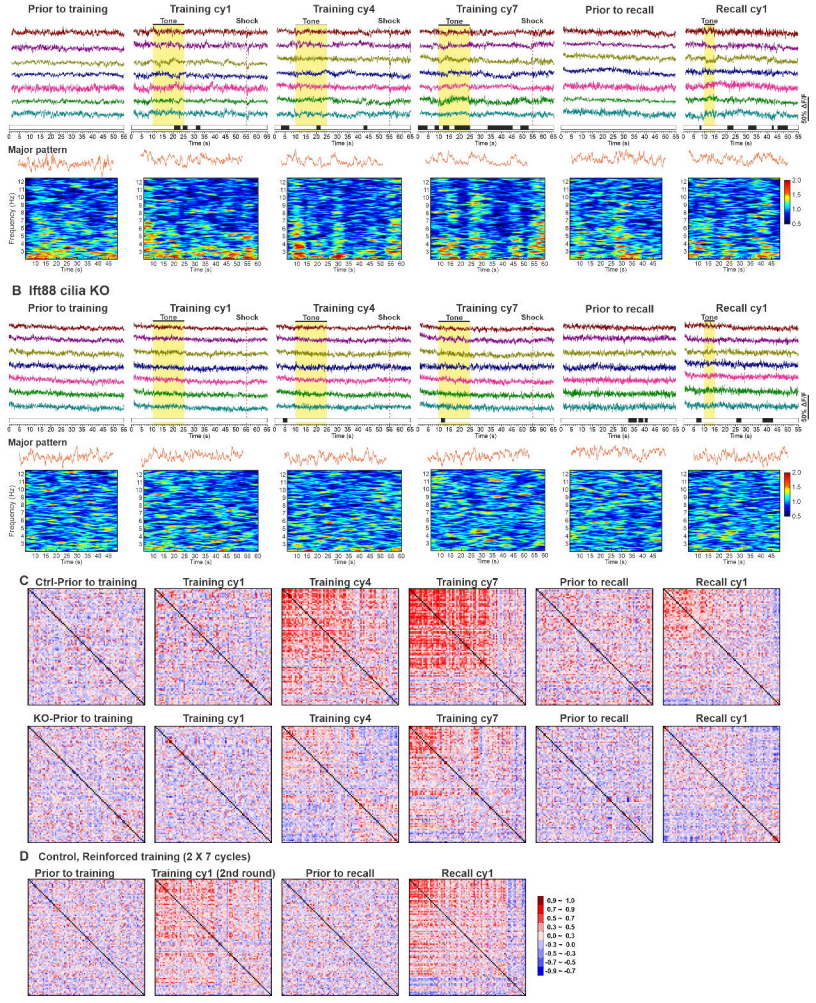
A Control
Prior to training
Training cy1
Training cy4
Training cy7
Prior to recall
Recall cy1
Tone
Shock
90% ΔF/F
Major pattern
Frequency (Hz)
Time (s)
B Ift88 cilia KO
C
Ctrl-Prior to training
KO-Prior to training
D Control, Reinforced training (2 X 7 cycles)
Training cy1 (2nd round)
0.9 ~ 1.0
0.7 ~ 0.9
0.5 ~ 0.7
0.3 ~ 0.5
0.0 ~ 0.3
-0.3 ~ 0.0
-0.5 ~ -0.3
-0.7 ~ -0.5
-0.9 ~ -0.7

Fig. 4

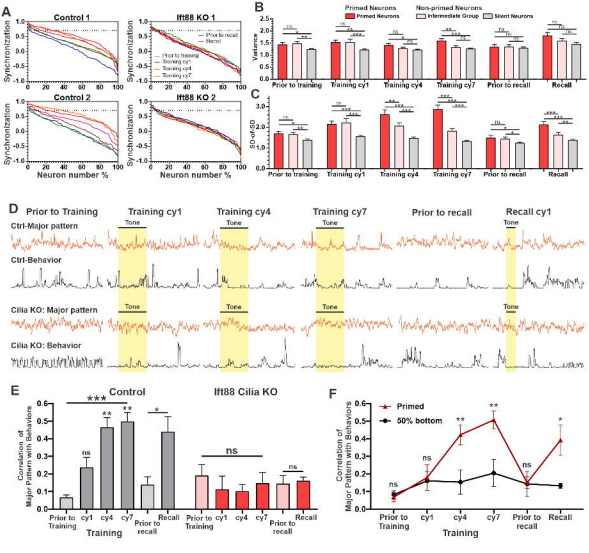
A
Control 1
Ift88 KO 1
Control 2
Ift88 KO 2
Synchronization
Neuron number %
Prior to recall
Recall
Training cy1
Training cy4
Training cy7
B
Primed Neurons
Non-primed Neurons
Primed Neurons
Intermediate Group
Silent Neurons
Variance
Prior to training
Training cy1
Training cy4
Training cy7
Prior to recall
Recall
C
SD-ratio
D
Prior to Training
Training cy1
Training cy4
Training cy7
Prior to recall
Recall cy1
Ctrl-Major pattern
Ctrl-Behavior
Cilia KO: Major pattern
Cilia KO: Behavior
Tone
E
Control
Ift88 Cilia KO
Correlation of Major Pattern with Behavioire
Prior to Training
cy1
cy4
cy7
Prior to recall
Recall
Training
ns
F
Primed
50% bottom
Correlation of Major Pattern with Behavioire
Training

Fig. 5

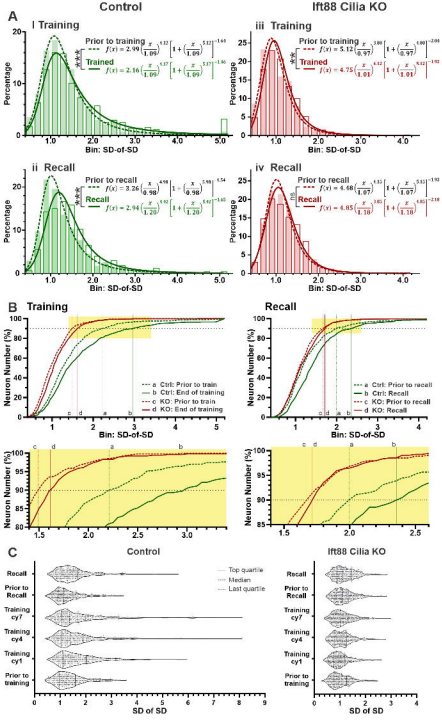
A
Control
Ift88 Cilia KO
i Training
iii Training
ii Recall
iv Recall
Prior to training
Trained
Prior to recall
Recall
Percentage
Bin: SD-of-SD
B
Training
Recall
Neuron Number (%)
a Ctrl: Prior to train
b Ctrl: End of training
c KO: Prior to train
d KO: End of training
a Ctrl: Prior to recall
b Ctrl: Recall
c KO: Prior to recall
d KO: Recall
C
Top quartile
Median
Last quartile
Recall
Prior to Recall
Training cy7
Training cy4
Training cy1
Prior to training
SD of SD

Fig. 6

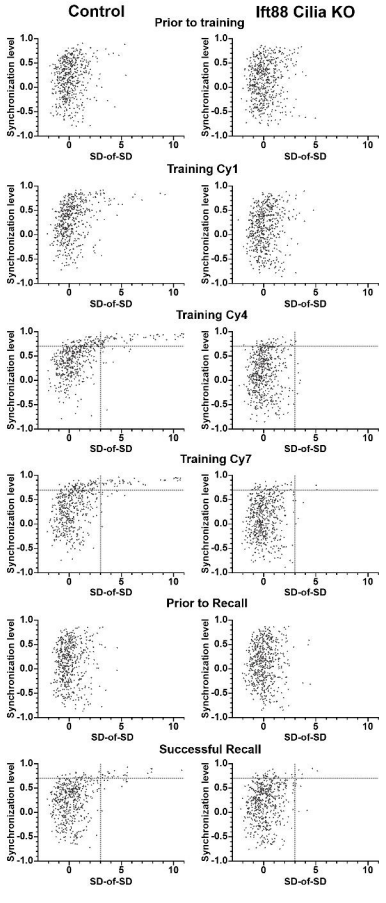
Control
Ift88 Cilia KO
Prior to training
Training Cy1
Training Cy4
Training Cy7
Prior to Recall
Successful Recall
Synchronization level
SD-of-SD
1.0
0.5
0.0
-0.5
-1.0
0
5
10

Fig. 7

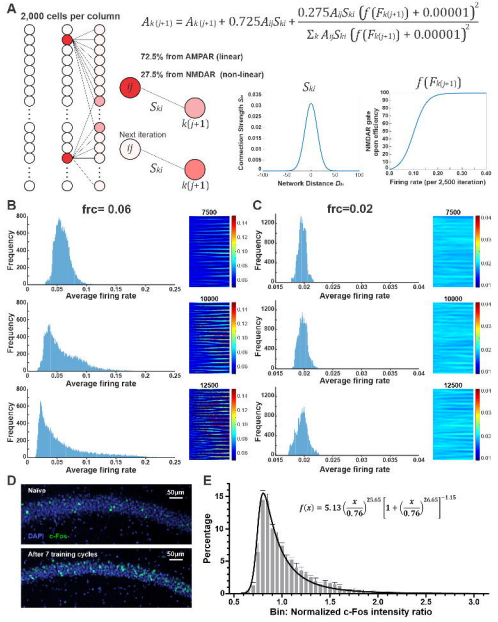
A
2,000 cells per column
$A_{k(j+1)} = A_{k(j+1)} + 0.725A_{ij}S_{ki} + \frac{0.275A_{ij}S_{ki}\left(f(Fr_{k(j+1)}) + 0.00001\right)^2}{\Sigma_k A_{ij}S_{ki}\left(f(Fr_{k(j+1)}) + 0.00001\right)^2}$
72.5% from AMPAR (linear)
27.5% from NMDAR (non-linear)
Next iteration
S_{ki}
$f(Fr_{k(j+1)})$
Connection Strength S_{ki}
Network Distance D_{ki}
NMDAR gate open efficiency
Firing rate (per 2,500 iteration)
B
frc= 0.06
C
frc=0.02
Frequency
Average firing rate
7500
10000
12500
D
Naïve
After 7 training cycles
50μm
DAPI
c-Fos
E
$f(x) = 5.13\left(\frac{x}{0.76}\right)^{25.65}\left[1+\left(\frac{x}{0.76}\right)^{26.65}\right]^{-1.15}$
Percentage
Bin: Normalized c-Fos intensity ratio

Fig. S1

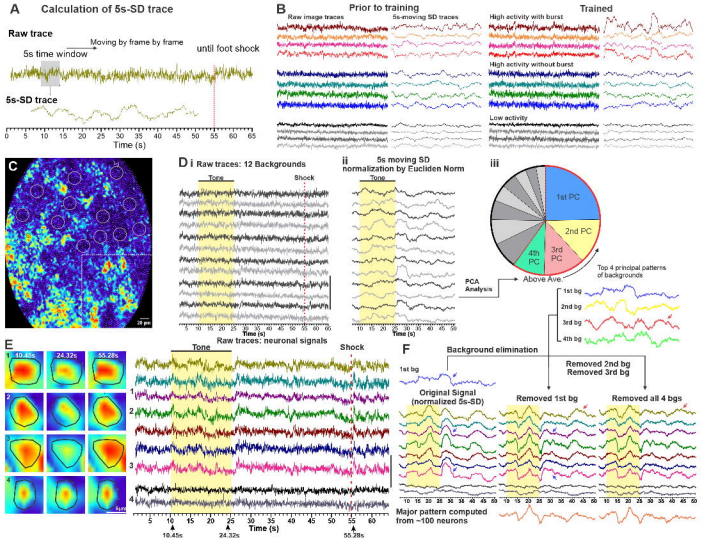
A
Calculation of 5s-SD trace
Raw trace
Moving by frame by frame
5s time window
until foot shock
5s-SD trace
Time (s)
B
Prior to training
Trained
Raw image traces
5s-moving SD traces
High activity with burst
High activity without burst
Low activity
C
D i Raw traces: 12 Backgrounds
Tone
Shock
Time (s)
ii
5s moving SD
normalization by Eucliden Norm
iii
1st PC
2nd PC
3rd PC
4th PC
PCA Analysis
Above Ave.
Top 4 principal patterns of backgrounds
1st bg
2nd bg
3rd bg
4th bg
E
Raw traces: neuronal signals
16.48s
24.32s
55.28s
Time (s)
F
Background elimination
1st bg
Removed 2nd bg
Removed 3rd bg
Original Signal
(normalized 5s-SD)
Removed 1st bg
Removed all 4 bgs
Major pattern computed
from ~100 neurons

Fig. S2

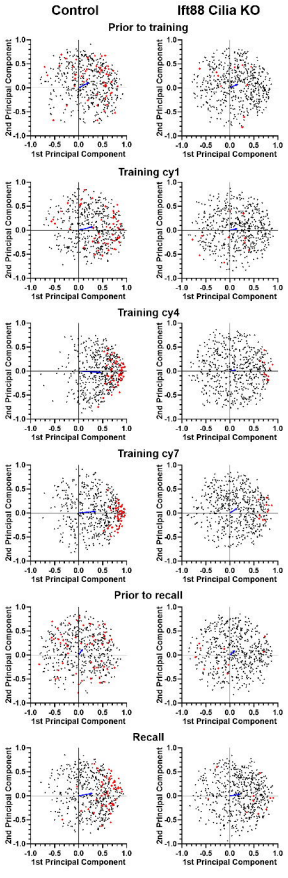
Control
Ift88 Cilia KO
Prior to training
Training cy1
Training cy4
Training cy7
Prior to recall
Recall
2nd Principal Component
1st Principal Component
-1.0
-0.5
0.0
0.5
1.0

Fig. S3

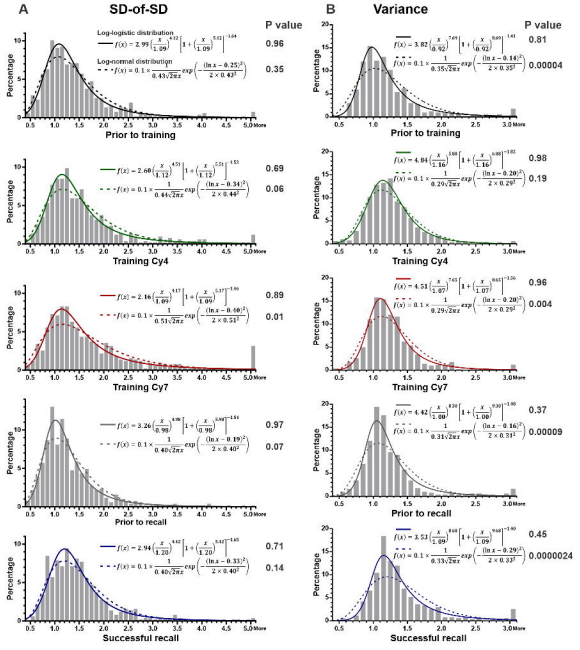
A
SD-of-SD
B
Variance
P value
Log-logistic distribution
Log-normal distribution
Percentage
Prior to training
Training Cy4
Training Cy7
Prior to recall
Successful recall
0.96
0.35
0.69
0.06
0.89
0.01
0.97
0.07
0.71
0.14
0.81
0.00004
0.98
0.19
0.96
0.004
0.37
0.00009
0.45
0.0000024